

**ALMA MATER STUDORIUM – UNIVERSITA DI BOLOGNA**

**SCHOOL OF ENGINEERING**

DEPARTMENT OF ELECTRICAL ENERGY AND INFORMATION ENGINEERING  
“GUGLIEMO MARCONI” (DEI)

MASTER DEGREE IN ELECTRICAL ENERGY ENGINEERING

**MASTER THESIS**

in

Technological Management of Electrical Infrastructures

**“Study of Electro-thermal Effects on PLA Materials Fed with AC  
Currents”**

---

STUDENT:

Olatunji Julius, Ojoawo

SUPERVISOR:

Prof. Andrea, Cavallini

CO-SUPERVISORS:

Dr. Juan Manuel, Martinez Tarifa

Dr. Ángel Manuel Gómez Solanilla  
(UC3M, ES)

Academic Year 2021/2022

Session II

## ABSTRACT

Given the rise in the emergence of new composite materials, their multifunctional properties, and possible applications in simple and complex structural components, there has been a need to unravel the characterization of these materials. The possibility of printing these conductive composite materials has opened a new area in the design of structural components which can conduct, transmit, and modulate electric signals with no limitation from complex geometry. Although several works have researched the behaviour of polymeric composites due to the immediate growth, however, the electrothermal behaviour of the material when subjected to varying AC applied voltage (Joule's effect) has not been thoroughly researched.

This study presents the characterization of the electrothermal behaviour of conductive composites of a polylactic acid matrix reinforced with conductive carbon black particles (CB-PLA). An understanding of this behaviour would contribute to the improved work in additive manufacturing of functional electro-mechanical conductive materials/structures with potential application in energy systems, bioelectronics, etc.

In this study, the electrothermal interplay is monitored under applied AC voltage, varying lengths, and filaments printing orientations (longitudinal, oblique, and transverse). Each sample was printed using the fused deposition modelling (FDM) technique such that each specimen has three different lengths. This makes a total of 9 samples - transverse, longitudinal, and oblique each with lengths 1L, 2L, and 2.75L. To this end, deductions were made on properties that affect composite material's efficiency and life expectancy in conductive structural components.

The result of this study shows a great influence of printing orientation on material properties of 3D printed conductive composites of CB-PLA. The result also identifies the drastic contribution of AC applied voltage to composites' stabilization time. This knowledge is important to provide experimental background for components' electrothermal interplay and estimate possible degradation and operating limits of composite structures when used in applications.

**Keywords:** Multifunctional, additive manufacturing, printing orientations, polylactic acid, carbon black.

## **DEDICATION**

My gratitude goes to my family, friends, and everyone who contributed to the success of this work.

I am esteemed to have been supervised by a man with vast experience and knowledge in Electrical Engineering, Dr. Juan Manuel Martínez Tarifa. His guidance, encouragement, corrections, and understanding through the course of this research have made it possible to achieve the project objectives set.

I also appreciate the contribution of Dr. Ángel Manuel Gómez Solanilla (at Universidad Carlos III de Madrid, Spain) and Prof. Andrea Cavallini (my supervisor at the University of Bologna, Italy) whose support and contributions have been helpful. I celebrate all the lecturers and professionals who have contributed to imparting knowledge to me throughout the course of my master's degree program.

I dedicate this work to you all. Thanks for your support.

## Table of Contents

<b>ABSTRACT</b> .....	<b>II</b>
<b>DEDICATION</b> .....	<b>III</b>
<b>INDEX OF FIGURES</b> .....	<b>VI</b>
<b>INDEX OF TABLES</b> .....	<b>IX</b>
<b>CHAPTER 1</b> .....	<b>1</b>
INTRODUCTION .....	1
1.1 Background .....	1
1.2 Problem Statement .....	1
1.3 Aim and Objectives.....	2
1.4 Significance of Study .....	3
1.5 Scope of Study .....	3
<b>CHAPTER 2</b> .....	<b>4</b>
STATE OF THE ART .....	4
2.1 Manufacturing Techniques.....	4
2.1.1 Traditional Manufacturing Process .....	4
2.1.2 Non-Traditional (Additive) Manufacturing Process.....	5
2.2 Polylactic acid (PLA) filled with Carbon Black (CB) Particles.....	6
2.3 Multifunctional Characterization Tests:.....	9
2.3.1 Thermo-electrical test .....	11
2.3.2 Mechano-electrical test.....	12
2.3.3 Electro-thermal test.....	13
2.4 Electrothermal Experimental Conditions .....	14
2.4.1 3D Characteristics and Microstructural Arrangement of Carbon Black .....	14
2.4.2 Resistance and resistivity variation .....	15
2.4.3 Joule Heating .....	18
2.4.4 Stability Criteria .....	21
2.5 Summary .....	21

<b>CHAPTER 3.....</b>	<b>22</b>
EXPERIMENTAL PROCEDURE .....	22
3.1 Preamble.....	22
3.2 Experimental targets.....	22
3.3 Sample description .....	22
3.4 Experimental Setup .....	24
3.4.1 Power supply unit.....	24
3.4.2 Measuring Units .....	25
3.4.2 Software and data analysis .....	28
3.5 Experimental Procedure .....	29
3.5.1 Composite heating and heating schedules .....	29
3.5.2 Stability Analysis.....	30
<b>CHAPTER 4.....</b>	<b>33</b>
RESULTS AND DISCUSSION.....	33
4.1 1L Samples.....	33
4.2 2L Samples.....	38
4.3 2.75L Samples.....	42
4.4 Resistive and thermoelectric response of tested CB-PLA .....	45
4.5 Stability and Stabilization Time.....	48
4.6 Influence of geometry on electrothermal response .....	50
<b>CHAPTER 5 .....</b>	<b>54</b>
CONCLUSION.....	54
REFERENCES.....	57
APPENDIX A .....	a
APPENDIX B .....	b
APPENDIX C .....	c

## INDEX OF FIGURES

2.1.	Scheme of the traditional manufacturing process of composites material.....	4
2.2.	Scheme of the additive manufacturing process of composites material.....	5
2.3.	Comparing the heating temperature of 3D printed honeycomb samples.....	7
2.4.	Effect of applied voltage on heating characteristics of composites with different carbon fiber concentrations.....	10
2.5.	Experimental setup for thermo-electric test on 3D printed conductive samples.....	12
2.6.	Experimental setup to investigate the influence of mechanical deformation on the resistance of 3D printed conductive samples.....	12
2.7.	Microstructure of the 3D printed CB-PLA with the conductive path.....	15
2.8.	Temperature against time showing the temperature evolution in three samples of 3D printed CB-PLA.....	16
2.9.	Resistance against temperature cure showing the evolution in three samples of 3D printed CB-PLA.....	17
2.10.	Finite element model for joule heating simulation in carbon fiber epoxy.....	19
2.11.	Schematic of the setup for Joule heating testing.....	20
2.12.	Surface temperature evolution with power and time during joule heating.....	20
3.1.	Verilec AC power source, type arc-4-2. (a) the front view. (b) top view. (c) back view.....	24
3.2.	Digital Multimeter.....	25
3.3.	Fluke Ti50FT-20 IR camera. (a) full kit. (b) screen.....	27
3.4.	Derivation of samples' average temperature from the analysis of thermal images using Fluke Connect.....	28
3.5.	SanDisk card reader connected to the laptop to analyze thermal images on Fluke Connect.....	29
3.6.	Flow chart of the electro-thermal experimental test.....	31
3.7.	Electro-thermal test for CB-PLA setup.....	32
3.8.	Equivalent circuit of the electro-thermal test setup for CB-PLA.....	32

4.1.	Experimental results for 1L samples heated by Joule effect imposing AC voltage 25V. These results are presented for transverse, oblique, and longitudinal samples. a.) Electric resistance is plotted against time. b.) Average temperature is plotted against time. c.) Maximum temperature is plotted against time.....	34
4.2.	Experimental temperature and resistance results for 1L samples heated by Joule effect, imposing AC voltages from 25V to 45V. a. transverse sample, b. oblique sample and c. longitudinal sample.....	37
4.3.	Experimental resistance and temperature results for 2L samples subjected to AC voltage 30V. These results are presented for transverse, oblique, and longitudinal samples. a.) Electric resistance is plotted against time. b.) Average temperature is plotted against time.....	38
4.4.	Experimental temperature and resistance results for 2L samples heated by Joule effect, imposing AC voltages from 30V to 80V. a. transverse sample, b. oblique sample and c. longitudinal sample.....	41
4.5.	Experimental resistance and temperature results for 2.75L samples subjected to AC voltage 30V. These results are presented for transverse, oblique, and longitudinal samples. a.) Electric resistance is plotted against time. b.) Average temperature is plotted against time.....	42
4.6.	Experimental temperature and resistance results for 2.75L samples heated by Joule effect, imposing AC voltages from 30V to 120V. a. transverse sample, b. oblique sample and c. longitudinal sample.....	44
4.7.	Experimental resistance and temperature results for composite samples subjected to AC voltage. a.) Electric resistance is plotted against average temperature in 30V/1L sample. b.) Electric resistance is plotted against average temperature in 60V/2L sample. c.) Electric resistance is plotted against average temperature in 90V/2.75L sample.....	46
4.8.	Experimental resistance and temperature results for 2L samples subjected to AC voltage 30V to 80V. These results are presented for transverse, oblique, and longitudinal samples. a.) Electric resistance is plotted against time. b.) Average temperature is plotted against time.....	47

- 4.9. Experimental resistance and temperature results for samples with a constant ratio of 25V/1L. This is to compare linearity and evaluate the contribution of sample length to the electrothermal behaviour of the composites. a.) Resistance vs. time. b.) Average temperature vs. time. c.) Maximum temperature vs. time.....51
- 4.10. Experimental resistance and temperature results for samples with a constant ratio of 30V/1L. This is to compare linearity and evaluate the contribution of sample length to the electrothermal behaviour of the composites. a.) Resistance vs. time. b.) Average temperature vs. time.....52

## INDEX OF TABLES

2.1.	Thermal properties of 3D printed honeycomb samples.....	7
2.2.	Surface resistance of 3D printed honeycomb samples.....	7
3.1.	Test samples dimensions and printing orientations.....	23
3.2.	Experimental steps of ac voltages imposed on composite samples.....	30

# CHAPTER 1

## INTRODUCTION

### 1.1 Background

Until the 1950s, traditional composites manufacturing processes were employed. This approach requires labour for assembling; it's time-consuming and capital intensive [1]. However, over the years, the non-traditional manufacturing process has revolutionized the field, replacing the traditional manufacturing techniques [2]. Due to the advent of technology, non-traditional manufacturing techniques have evolved into 3D printing/additive manufacturing techniques. This has created opportunities for the customization of several structural composites components in the new generation industry. In this regard, new materials are emerging to provide diverse functionalities while maintaining some structural functions. Another limitation of the traditional manufacturing technique was the manufacturing of composites with complex geometries and heterogenous electro-mechanical properties. 3D printing techniques have overcome this challenge. Several techniques can also be used to manufacture these complex composites, and a typical example is Aerosol Jet printing[3].

In recent times, there has been a necessity for an in-depth background study of the emerging multifunctional materials. These materials are proposed to find applications in biosensors, energy storage systems, and wearable electronics. A typical example is the conductive polymeric composites [CPCs] which could find application in systems where electrical current flow is required in mechanical components. This material is a great substitute for conventional conductive material.

### 1.2 Problem Statement

In manufacturing conductive structural components, one limitation has been the material's strength while subjected to very high electrical, thermal and mechanical stresses. However, conductive thermoplastic exhibits a property that makes it one of the best solutions to this challenge. Conductive thermoplastic of polylactic acid filled with conductive carbon black

particles is made up of thermoplastic matrix (PLA matrix) reinforced with carbon black to create a conductive path within them.

In addition, fused deposition modelling (FDM) is an effective technique used to manufacture these thermoplastics. Although these printed composites have a lot of advantages, there are several complexities associated with the manufacturing process and microstructural compositions. A typical example is characterizing materials' conductivity. From percolation theory, it has been hypothesized that materials conductivity depends on the shape, size of conductive particles, fillers aspect ratio, and dispersion of fillers within the matrix. Percolation theory accounts for the creation and destruction of conductive pathways.

Recent works of literature have examined the multifunctional responses of 3D printed conductive polymeric composites, focusing on the electro-mechanical behavior of these materials when utilized as strain sensors, force sensors, or flex sensors, getting the variation in resistivity as they get deformed or degraded. Graphene/PLA honeycomb structure [4], carbon fiber-epoxy [5] composites, polyvinyl [6] acetate with graphite adhesive, and other composites have been considered in similar works. The thermo-electrical behaviour of the above-listed composites was researched; however, the stress type introduced was not induced by applied AC voltage (indirect heating). These works subjected the filaments to direct heating through the thermal chamber. Also, most of these works didn't present a specific analysis of the relationship between the evolution of resistance with temperature and thermal stability between voltage-power steps, nor was the stability criterion properly defined.

### **1.3 Aim and Objectives**

This work aims to study the electrothermal behaviour of 3D printed conductive PLA composites reinforced with conductive carbon black particles when subjected to applied AC voltage.

#### **Objectives**

1. To unravel the composite's response when subjected to low and high AC voltage.

2. To evaluate the contribution of three printing orientations (transverse, longitudinal, and oblique) to composites' electrothermal behaviour.
3. To evaluate the contribution of geometry (length) to the electrothermal behaviour. This will give information about linearity in the sample's behaviour.
4. To provide experimental background for components electrothermal interplay and estimate possible degradation and operating limits of composite structures when used in applications.

#### **1.4 Significance of Study**

A major gap in previous works is the analysis of the electrothermal response over time. An understanding of this interplay would help to unravel materials behaviour and predict mechanical aging when subjected to continuously applied AC voltage.

Working on this project is an opportunity to acquire knowledge in material science and its interdisciplinary relationship with energy engineering. Beyond these gains for the student, the project intends to contribute to an improved work in additive manufacturing in functional electro-mechanical materials/structures with potential application in energy systems, bioelectronics, etc.

#### **1.5 Scope of Study**

This study will research and analyze the electrothermal properties of 3D CB-PLA conductive composite materials with three printing orientations. The sample lengths and imposed AC applied voltage would be varied to unravel the electrothermal interplay. An in-depth study of the material's behavior when exposed to high AC electrical potential is important to make progress in the field of multifunctional conductive structures

The results of this work will contribute to ongoing research in composites material structures, giving experimental background for the degradation of devices and exploring their future applications and operating limits.

## CHAPTER 2

### STATE OF THE ART

#### 2.1 Manufacturing Techniques

Manufacturing is fundamental for the generation of wealth, industrialization, and developments in the quality of life [7]. Manufacturing complexities involve - system design, organization, technological logistics, operational planning, and control. Manufacturing techniques could be classified as traditional manufacturing processes and non-traditional manufacturing processes. The traditional processes had been in existence before 1950, while the non-traditional process has been implemented since the 1950s [7].

##### 2.1.1 Traditional Manufacturing Process

This is a conventional way of manufacturing composites. It involves manufacturing each part of a composite material separately - removing material from larger stock before assembling to form the desired shape. This approach is expensive, requires labor for assembling [1], and involves complex supply chains resulting in high cyclic times and long production runs [8], [9]. The manufacturing process is one of the primary factors limiting the development of novel smart components. Traditional casting and extruding procedures [10] have several constraints when it comes to complex shapes and heterogeneous electro-thermal-mechanical properties. These are addressed by introducing additive manufacturing or 3D printing techniques [2]. A schematic view of traditional manufacturing is shown in Figure 1.

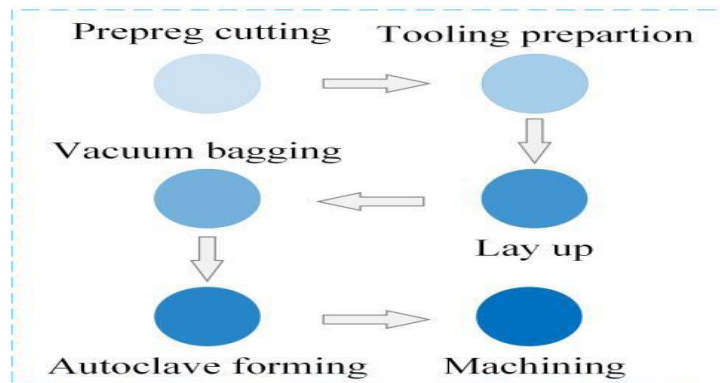


Fig. 2.1. Scheme of the traditional manufacturing process of composites material [11].

### 2.1.2 Non-Traditional (Additive) Manufacturing Process

The additive manufacturing (AM) process, also known as the three-dimensional (3D) printing technique, has transformed the industry, substituting traditional manufacturing methods [2]. AM, as defined by the ASTM society, is a layer-by-layer method of combining or adding materials together with the goal of creating composite material/object from 3D model data [7]. Decentralization is arguably the most significant distinction between additive and traditional production. Additive manufacturing can be done locally rather than in huge, centralized companies with 3D printing equipment. As a result, manufacturers can lower production costs, shorten their supply chains, and create complex geometries [1]. Amongst the possibilities presented due to the printing advancements in the last decades include applications in bioelectronics, robotics, automobiles, medical implants, and wearable devices based on conductive polymers [2]. Srivatsan and Sudarshan [7] discussed additive manufacturing of materials, viable techniques, advantages, and applications.

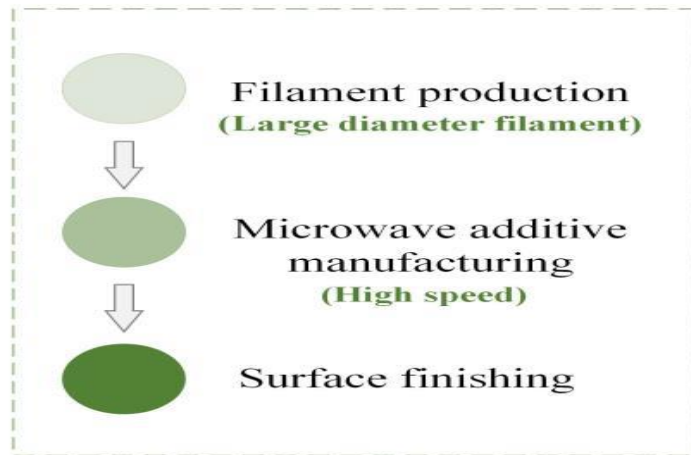


Fig. 2.2. Scheme of the additive manufacturing process of composites material [11].

Although additive manufacturing techniques have enabled design versatility, coupled with providing ways to customize structural components [2], the present challenge is optimizing structural functions and manufacturing new materials with interplayed multifunctional properties. Several works have investigated the properties of polymeric composites [2] and their accompanying fillers, with few considerations of the electro-thermal-mechanical behavioral interplay. Motivated by previous works, this study takes advantage of existing research works and focuses on the electrothermal behavior and properties of 3D printed

polymeric composites of polylactic acid (PLA) filled with carbon black conductive particles supplied with AC voltage. The use of conductive particles within the polymer matrix enables programmable control of the multifunctional properties (electro-thermal-mechanical response) [2]. The findings of this study will contribute to improving additive manufacturing in functional electro-thermal components [2] and progress in the potential usage of the 3D printed conductive polymers. These multifunctional conductive polymers are a great substitute for conventional conductive materials - for applications in flexible electronics [12], energy harvesters, soft robotics, biosensors [8], composite sensors, electrical circuits [9], thermoelectric elements, and 3D electrodes [13][14][15][16][17], smart biomaterial, healthcare, and biomedical devices [15-18].

## **2.2 Polylactic acid (PLA) filled with Carbon Black (CB) Particles**

Recent works have researched the characterization of polymeric composites. Kim et al. [4] analyzed the characterization of electrical heating of Graphene (GR)/PLA honeycomb structure composite manufactured by conveyor fused deposition modelling (CFDM) 3D printer. Three types of filaments were analyzed for 3D printing – PLA, CB/PLA, and GR/PLA. Results of the thermal analysis show that they all presented different thermal peaks, with the thermal peak in CB/PLA being the highest.  $T_m$  (melting temperature) increased in CB-PLA and GR/PLA as they showed more crystalline regions; the former shows a larger crystalline region due to the nucleation effect of carbon fillers. The thermal peaks demonstrated during heating include  $T_g$  (glass transition temperature),  $T_{cc}$  (cold crystallization temperature), and  $T_m$  (melting temperature).

**$T_{cc}$  (cold crystallization temperature)** - Temperature at cold crystallization and the crystalline phase transition region from crystal induced when CB and GR are added to PLA.

**$T_m$  (melting temperature)** - Temperature during melting of a large portion of crystals in composites. These portions are formed due to the nucleation effect of carbon nanofillers.

**$T_g$  (glass transition temperature)** - The temperature at the region where the polymeric chain of the composites presents high mobility translating into a large increase in the resistance to temperature ratio (resulting in a steeper slope).

TABLE 2.1. THERMAL PROPERTIES OF 3D PRINTED HONEYCOMB SAMPLES [4].

Temperature	Material		
	PLA	CB-PLA	GR-PLA
T <sub>g</sub> (°C)	59.3	61.9	44.2
T <sub>cc</sub> (°C)	99.6	98.2	70.3
T <sub>m</sub> (°C)	156.7	166.2	163.8

In addition, Kim et al. [4] applied a constant DC voltage to the samples and compared the surface resistance and temperature of these samples, which were both in the machine direction (direction aligning with the forward direction of the composite during printing) and cross direction (direction which is perpendicular to the machine direction).

Fig. 2.3 shows the plot of the electrical heating temperature of carbon black against applied DC voltage. The temperature evolution of the sample in machine direction (MD) is higher than that of the sample in cross direction (CD).

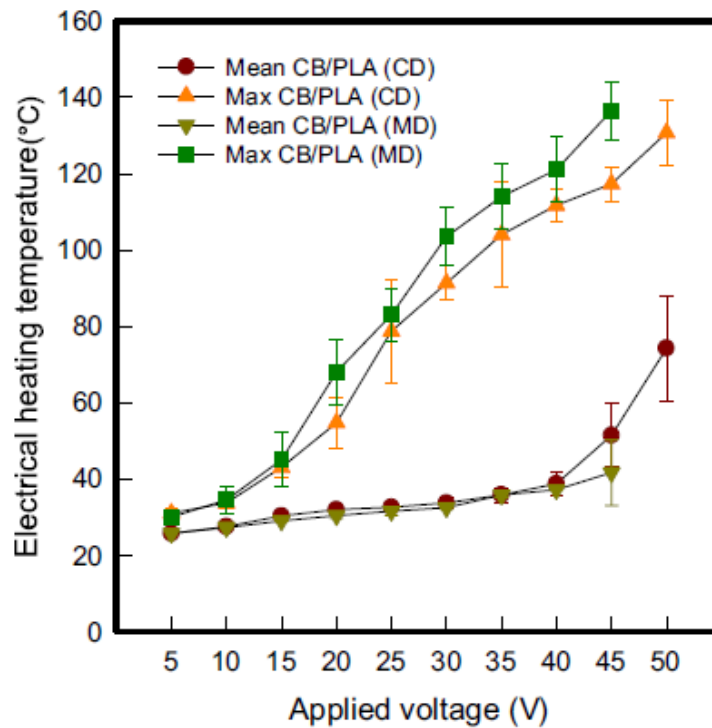


Fig. 2.3. Comparing the heating temperature of 3D printed honeycomb samples [4].

The surface resistance in the machine direction is higher than that in the cross direction, as shown in table 2.2. below.

TABLE 2.2. SURFACE RESISTANCE OF 3D PRINTED HONEYCOMB SAMPLES [4].

<b>Direction</b>	<b>Resistance (<math>\Omega</math>/sq)</b>		
	<b>PLA</b>	<b>CB-PLA</b>	<b>GR-PLA</b>
<b>Cross Direction</b>	$>10^{13}$	$299.0 \pm 14.6$	$118.0 \pm 15.9$
<b>Machine Direction</b>	$>10^{13}$	$371.7 \pm 50.3$	$129.8 \pm 37.8$

PLA (polylactic acid) material is a thermoplastic aliphatic polyester produced by direct condensation polymerization of lactic acid or by ring-opening polymerization of lactide [18]. PLA is derived from biodegradable and renewable resources; the degradation products are non-pollutant and non-toxic. PLA has attracted great interest from industries, research, and 3D printing using FDM, which is related to availability and some characteristics that are lacking in other polymers, such as renewability, biocompatibility, processability, and energy-saving [19].

Although PLA presents lots of prospects, its use has some shortcomings - poor chemical modifiability (absence of readily reactive side-chain groups), mechanical ductility [20], and cost [21]. Some approaches are employed to alleviate these challenges - blending PLA with other polymers[22]–[29], functionalization [30]–[34], and addition of nanofillers [35], [36]. The introduction of nano fillers is an interesting approach since, with little quantity of fillers, it is possible to optimize the desired features without altering PLA’s main properties. Amongst the commonly used nanofillers are Nano-clays [37]–[45], Nano-silicas [35], [46], [47], and Carbon nano-based materials [36], [48]–[53].

According to Ladani et al. [54], carbon nanomaterials have different electrical properties depending on their printing orientation. Carbon black is one of the most used nanomaterials as polymer fillers and rubber reinforcement due to its high surface-to-volume ratio and versatility [2]. A study by Kim et al. [4] states that carbon black has a good thermal property upon characterization of carbon materials using Raman spectra. Carbon black particles are produced by partial combustion and pyrolysis of low-value oil residues at high

temperatures under regulated process conditions. This material has good conductive characteristics. The central physical and chemical properties of CB include particle size, porosity, structure, and surface chemistry. These properties are distributional in nature, and this distribution affects performance. In line with the above, because of these characteristics, CB particles combine well when used as fillers in a polymeric matrix, forming conductive pathways within the composite [5], [55].

This study takes advantage of existing works [2], [4], using the commercial polylactic acid reinforced with carbon black to make the fused deposition modelling (FDM) 3D printed composites material whose electro-thermal behavior would be investigated:

- The polymeric matrix of PLA 4043D.
- 53% of CB by mass.
- CB Volume: 26.5% and median particle size by volume of 224  $\mu\text{m}$  [55].

In addition, the polymeric filaments with carbon black (CB/PLA) as filler is cheap and easily available.

### **2.3 Multifunctional Characterization Tests:**

As described earlier, the conductive polymeric composite material to be studied provides multiple electrical properties; this makes it a solution in the design of structural components which finds applications in diverse industries (automobile, electrical, etc.). Due to the advent of 3D printing technologies, recent works of literature have examined the multifunctional responses of 3D printed conductive polymeric composites, focusing on the electro-mechanical behavior of these materials when utilized as strain sensors, force sensors, or flex sensors, getting the variation in resistivity as they degrade. Graphene/PLA honeycomb structure [4], carbon fiber-epoxy [5] composites, polyvinyl [6] acetate with graphite adhesive, and other composites have been considered in similar publications. However, most of these works didn't present a specific analysis of the relationship between the evolution of resistance with temperature, thermal stability between voltage-power steps, nor the stability criterion was defined.

It is well known that current flow through a conductive material leads to a heating process governed by the Joule Effect [2]. Joule heating occurs when voltage is applied to a material; current flows through the conductive material, and it gets heated due to an increase in its internal energy. This thermal response due to the Joule effect affects the electrical and mechanical behavior of the conductive polymeric composites (CPCs), and this results in the thermo-electro-mechanical interplay. If the electrical heating process is created by a constant voltage level, the relationship between dissipated heat and voltage is given thus:

$$Q_{dissip} = \int_0^t \frac{V^2}{R} dt \quad (2.1)$$

$V = Applied\ voltage$

$R = Electric\ Resistance$

$Q_{dissip} = Dissipated\ Heat$

M. Kim et al. [5] performed the resistive heating test and showed the resistive heating increased proportionately with respect to the applied constant voltage in composite samples with different carbon fibers (CFs) concentrations (1, 3, 5 weight wt.%). This is shown in Fig. 2.4.

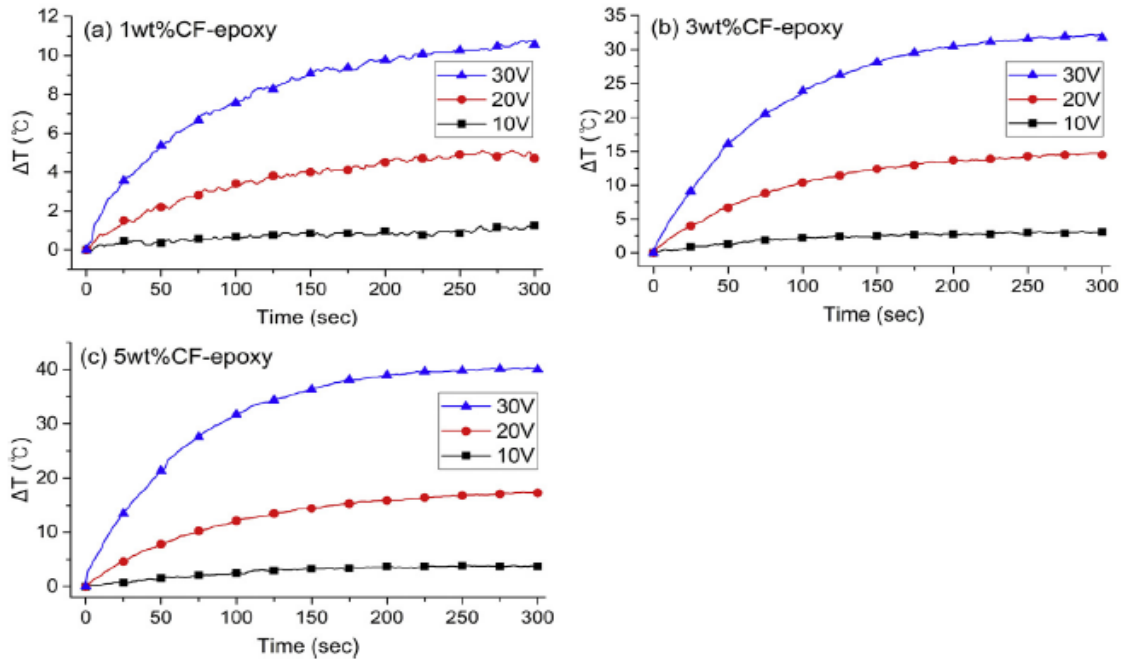


Fig. 2.4. Effect of applied voltage on heating characteristics of composites with different carbon fiber concentrations [5].

I.Tirado-Garcia et al. [2] investigated the interplays of mechanical, electrical, and thermal effects on 3D printed polymeric composites of polylactic acid (PLA) filled with carbon black (CB) conductive particles and conducted mechanical characterization of PLA 4043D and CB-PLA specimens printed in longitudinal filaments orientation. Also, some works such as [4]–[6], [28], [56] have investigated the multifunctional characterization of conductive polymeric composites.

The multifunctional characterization includes:

1. Thermo-electrical test
2. Mechano-electrical test
3. Electro-thermal test

### **2.3.1 Thermo-electrical test**

The goal of this test is to analyze the influence of temperature on the resistance of the 3D printed conductive polymeric composites (CPCs). A study by [2] monitored the evolution of the DC resistance with respect to the temperature field. In this work by [2], sample lengths were fixed; however, the filament orientations were changed to have three samples of the same length but different printing orientations - longitudinal ( $0^\circ$ ), transverse ( $90^\circ$ ), and oblique ( $\pm 45^\circ$ ).

The 3D printed CB-PLA samples were subjected to heat inside a thermal chamber till the desired temperature value was reached. The temperature was monitored using the chamber's thermocouple and by another thermocouple positioned close to the samples to maintain homogeneous conditions within the chamber. Three conventional ohmmeters were then used to measure the DC resistance of the three samples. Since these measuring devices use quite low voltage levels, heating in this experiment comes from external sources and not from Joule's effect. It was observed that the longitudinal sample presents a lower resistance value, with oblique being intermediate and transverse with a high resistance value. The experimental setup for the thermo-electric test by [2] is presented in Fig. 2.5.

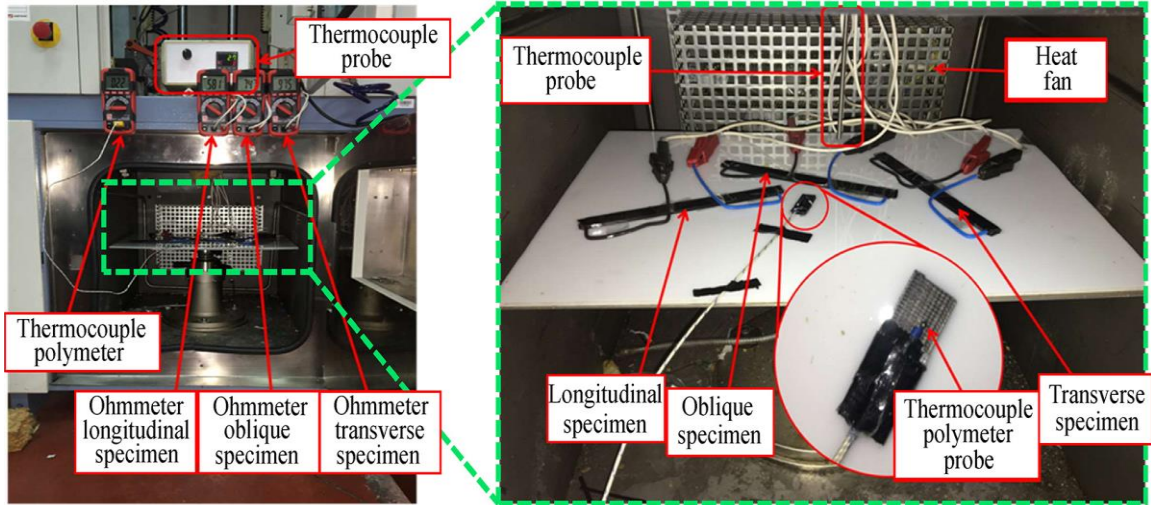


Fig. 2.5. Experimental setup for thermo-electric test on 3D printed conductive samples [2].

### 2.3.2 Mechano-electrical test

This test involves the analysis of the effect of mechanical deformation on the samples' electrical resistance. It was hypothesized that the deformation of the composites would produce the formation of new conductive electric paths. Furthermore, to evaluate the mechano-electric coupling, the longitudinal samples are better for the experiment as they provide the best thermo-electrical response due to their homogeneity. Fig. 2.6. depicts the setup used to track the progression of stress and electrical resistance as a function of mechanical (structural) deformation [2].

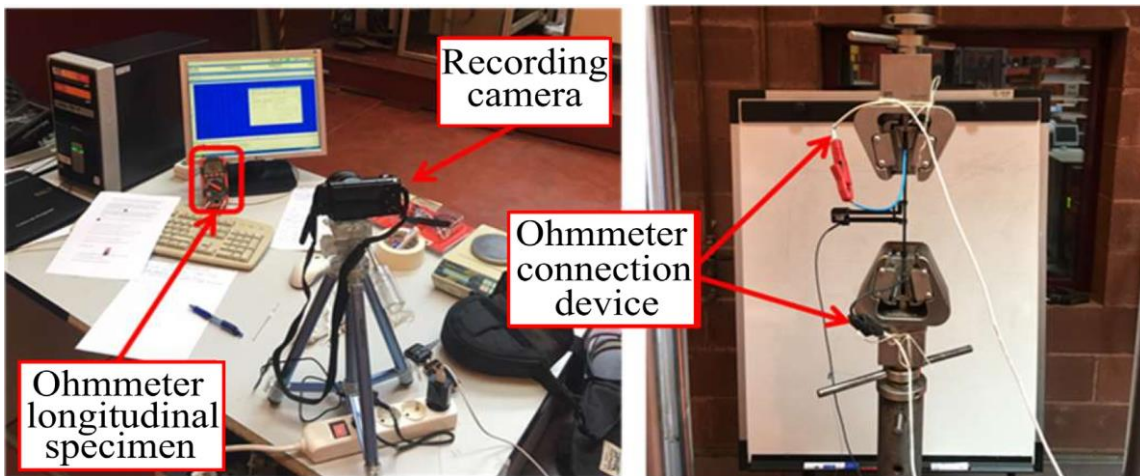


Fig. 2.6. Experimental setup to investigate the influence of mechanical deformation on the resistance of 3D printed conductive samples [2].

### 2.3.3 Electro-thermal test

Amongst the few works of literature that have investigated the electrothermal interplays of polymeric composites made from thermoplastic materials filled with conductive particles (filler), polymers such as High-density poly ethylene (HDPE) [6], [57], [58], Polyvinylidene fluoride or polyvinylidene difluoride (PVDF) [6], [59], polypropylene (PP), epoxy [60], and nylon, have been filled with Carbon Black (CB) [56], [61], [62] carbon fiber [59], graphene [11], Multiwall Carbon Nanotube (MCNT) [63].

However, direct heating (by heating element) has been used to study this relationship [56], but only a few articles have introduced indirect heating (from the Joule Heating Effect or Hall Effect tests [11]) to study the variation of temperature with electrical resistivity or vice versa. As earlier described, the Joule heating effect leads to the generation of temperature when current flows through a conductive material. In addition, when the electrical field is high enough, the generated heat can experience a rise in temperature above the glass transition temperature ( $T_g$ ), which can lead to changes in the electrical behaviour of the sample. Thus, it is important to study the conductivity of the composite and analyze the electrical behavior due to the creation or destruction of conductive paths [2].

During the electro-thermal test, heat is supplied indirectly to the composite via current flow in the conductive composite. A constant voltage is applied to the composite samples, and the temperature evolution is monitored using the infrared camera (IR). Two output variables can be obtained with this camera and certain analytical software; these are the maximum temperature ( $T_{max}$ ) at the surface of the sample at an instant time and the average temperature ( $T_{avg}$ ), which represents the average of the temperature distribution along the sample's surface at an instant time. I. Tirado Garcia et al. [2] earlier carried out this test using the DC voltage source on the printed conductive specimen and discussed the potential inhomogeneities in samples' temperature distribution. Once the stabilization criteria are met with reference to the  $T_{max}$  and current value between two instant times, the voltage level is raised to study the effect of increasing the generated heat in the sample. This criterion is an important experimental condition that will be further explained in a subsequent chapter.

This research will focus on the electro-thermal properties of 3D printed CB-PLA conductive composites. An in-depth understanding of the electro-thermal response with respect to time would help to unravel the electro-thermal behaviour of materials when the composite is used in conductive structural devices and exposed to continuous electric conduction. Furthermore, this work will take advantage of existing works and explore electro-thermal experimental conditions.

## **2.4 Electrothermal Experimental Conditions**

To establish a complete electric and thermal response [2] of the composite material over time, two magnitudes are measured: the average temperature ( $T_{avg}$ ) and the resistance of the specimen. In doing this, composites' geometrical features and other listed experimental conditions are needed for better characterization analysis.

- I. 3D (dimensional) characteristics:
  - a. Printing Orientation.
  - b. Dimension's selection - sample's length variation.
- II. Resistance and resistivity variation.
- III. Joule heating.
- IV. Stability Criteria

### **2.4.1 3D Characteristics and Microstructural Arrangement of Carbon Black**

Voids are major defects that affect the conductivity of composite structures. Voids are pores in a composite material. These pores are unfilled with polymer or fiber [64]. Voids are the results of a poor manufacturing process; for this reason, the manufacturing process and printing of composites are given appropriate consideration. A reduction of voids increases conductivity irrespective of the printing orientation. These two parameters: printing orientation and length, are key in voids' distribution and quantity. The microstructure arrangement of carbon black within the polymeric matrix defines the nature of the conductive behavior of 3D printed conductive composites (CB-PLA). In this regard, conductive paths are defined by the formation of conductive paths between filaments

(sintering process) and placement of the carbon black in the filaments either at filament level or inter-filaments level. This property is due to the dielectric characteristic of the polymeric matrix. In addition, the formation of these conductive paths guarantees the suitability of the conductive composites and the influence of printing orientation. The microstructure of the 3D printed CB-PLA is shown in Fig. 2.7 below.

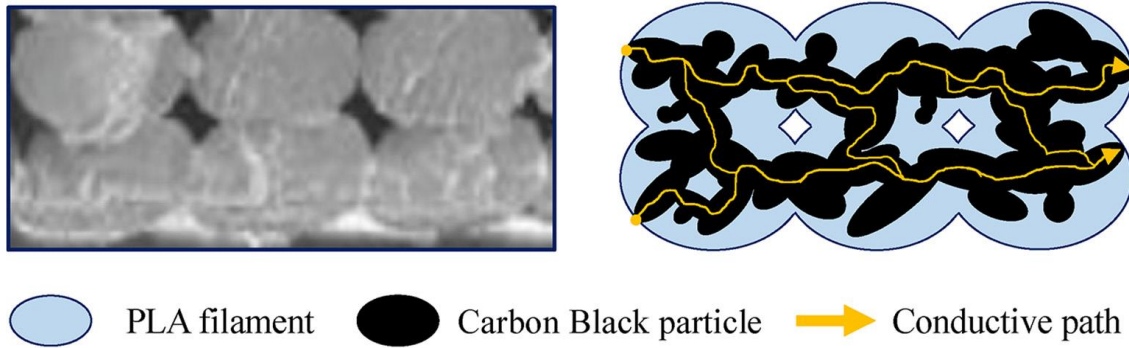


Fig. 2.7. Microstructure of the 3D printed CB-PLA with the conductive path [2].

This present work would have similar analyses for the same sample type accounting for three printing orientations as mentioned earlier, nonetheless, with varying sample lengths. The printing orientation would help to monitor the temperature evolution with respect to the printing. In addition, homogeneity/heterogeneity of each sample type and varying the sample length give better insight into the interplay of the composite's response.

#### 2.4.2 Resistance and resistivity variation

Electrical resistance is defined as a measure of the opposition to the flow of current in an electric circuit [65]. When a potential difference is applied across a conductor, current flows, and as a consequence, there exists high electrons' mobility. These free electrons collide with the fixed atoms, which form the static molecular structure of the conductor. As the collision continues, the rate of flow of electrons is inhibited. This restriction is the opposition called 'resistance of a conducting material.'

Mathematically, it could be expressed as

$$R = \rho \frac{L}{A} \quad (2.2)$$

Where:

$R$  = Resistance of the conductive material measured in Ohms

$L$  = Length of the conductive material

$A$  = Cross sectional area of the conductive material

$\rho$  = Resistivity of the material

According to equation (2.2), besides the relative displacements of the conductive particles, it is expected that a change in the specimen's length/cross-section area would contribute to a change in the specimen's electrical resistance. [2] confirmed that the resistance in oblique and transverse specimens is subjected to the dispersion of conductive particles' aggregates and the sintering process which occurs during the formation of other conductive paths between filaments (i.e., inter-filaments conductive paths). A constant voltage of 30 volts is applied to the specimens; the result of this work showed that specimen with low resistance has higher temperature at an instant time, which agrees with the increase in heat generated (see equation (2.1)). Fig 2.8. shows the temperature evolution at 30 volts (constant applied voltage); the figure shows the longitudinal sample having the highest temperature value, transverse with a low value, and oblique being intermediate.

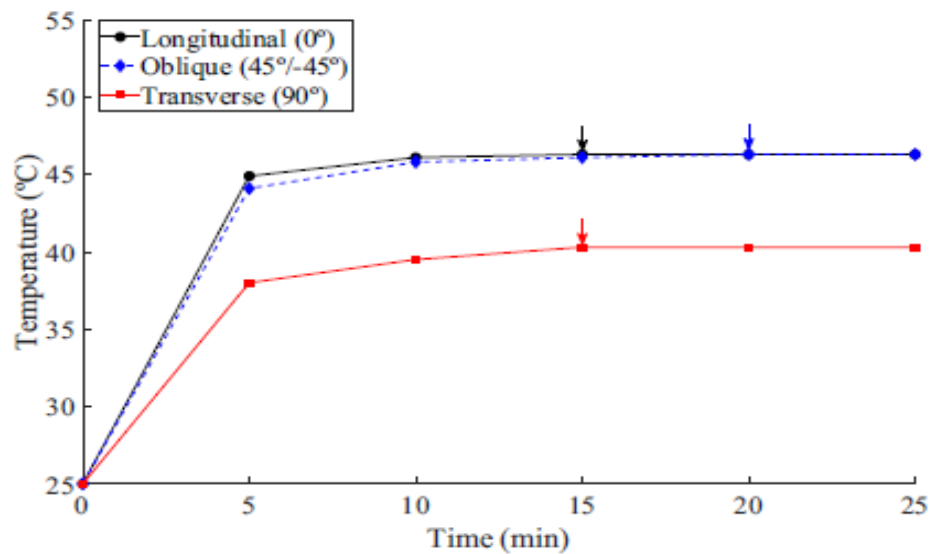


Fig. 2.8. Temperature against time showing the temperature evolution in three samples of 3D printed CB-PLA [2].

Figure 2.9 compares the samples' measured DC resistance values at 30 volts (constant applied voltage) with applied temperature values. The longitudinal sample shows lower resistance, followed by oblique and transverse specimens [2].

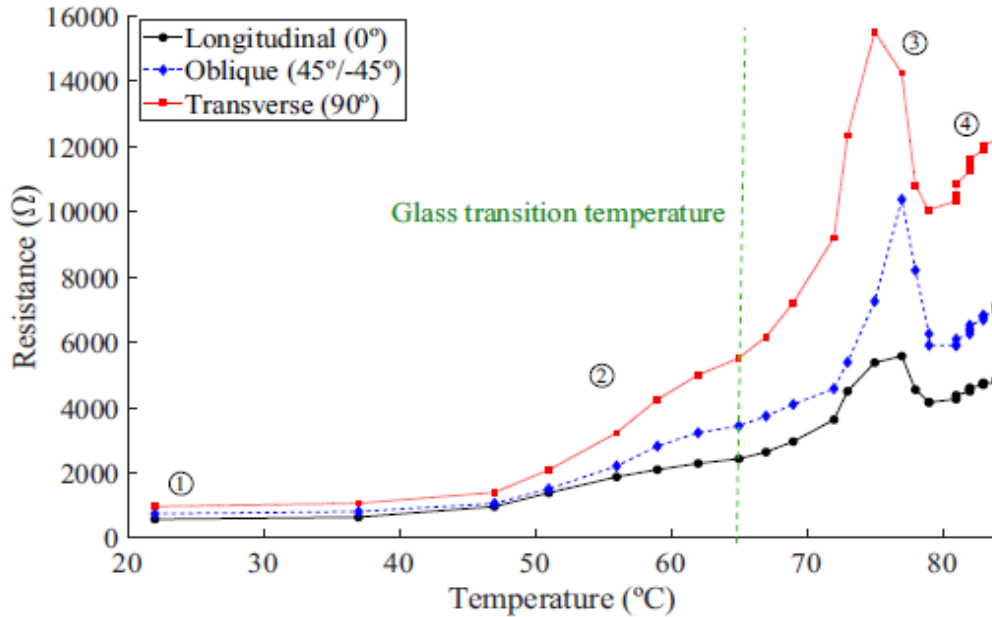


Fig. 2.9. Resistance against temperature cure showing the evolution in three samples of 3D printed CB-PLA [2].

Results of Fig. 2.8 and 2.9 were consistent with the consequence of Joule's effect in section 2.3. This study takes advantage of ohm's law [65] (the current flowing between two points in a conductor is directly proportional to the voltage to resistance ratio across the conductor) to compute the current flow through each sample mathematically, having obtained the DC resistance value using ohmmeter, as shown in equation (2.4)

$$I = V/R \quad (2.4)$$

Where:

$R$  = Resistance of the conductive material measured in Ohms

$V$  = Applied voltage across the conductive material

$I$  = Current flowing through the conductive material at specific period

Kim et al. [4] also investigated the electrical heating performance of Carbon black/PLA and graphene/PLA honeycomb based on the surface temperature at various applied constant voltages (DC). The resistance  $R$  of the sample was obtained using a multimeter, and the calculate the surface resistance, two parallel electrodes were connected to each end of the sample. The surface resistance ( $R_s$ ) was thus calculated afterwards as shown in equation 2.5.

$$R_s = \frac{W}{D} \times R \quad (2.5)$$

Where:

$R_s$  = Surface resistance, measured in  $\Omega/\text{sq}$

$R$  = Measured resistance, measured in  $\Omega$

$W$  = Width of the sample.

$D$  = Distance between the two electrodes

### 2.4.3 Joule Heating

As earlier described in section 2.3, Joule heating occurs when voltage is applied to a material; current flows through the conductive material, causing heat. This phenomenon is represented by equation 2.1.

M. Kim et al. [5] define Joule heat  $Q$  as the energy converted from electrical energy to thermal energy. The effect of fiber contact on joule heating was investigated by varying the distances between fibers. According to [5], joule heating in discontinuous carbon fiber epoxy composites originates from the formation of a 2D conducting network by electrically conducting carbon fibers (CFs). This network includes conducting fillers and contacts between the fillers. The contacts between the carbon fibers and networks are critical for heating efficiency analysis. The results of this study by [5] earlier described in figure 2.4. shows a proportionate increase between the applied voltage, carbon fiber concentration, and heating behavior which agrees with Joule's first law.

Finite element analysis (FEA) was introduced to analyze the relationship between the applied voltage, geometry, and heating response. The result of this analysis, increasing the contacts with increased carbon fiber concentration, confirmed that higher temperatures could be obtained at higher carbon fiber volume fractions. This result also agrees with the Joule heating principle. Details about this model can be found in [5]. Figure 2.10 represents the finite element model used for joule heating simulation.

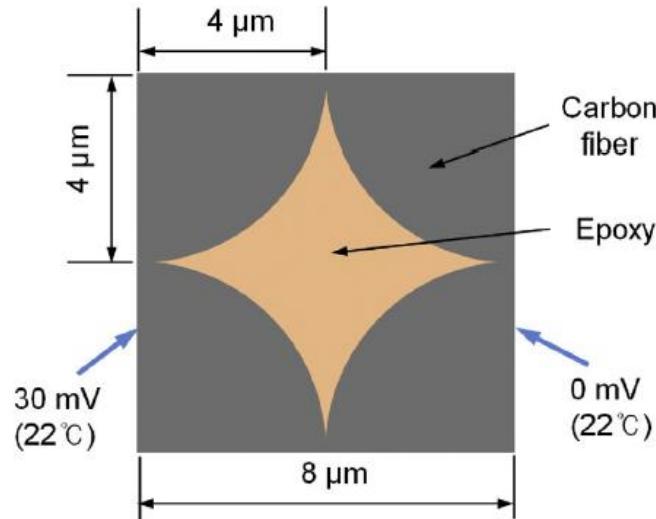


Fig. 2.10. Finite element model for joule heating simulation in carbon fiber epoxy [56]

In another research, R. Taherian et al. [56] performed a hall effect test and joule effect test on polyvinyl acetate polymer filled with graphite (PVAC/G). The behaviors of the negative temperature coefficient (NTC) and positive temperature coefficient (PTC) of this adhesive were monitored. The test result shows that the Joule effect has more impact on fillers' alignment due to high electric field strength. To perform the Joule heating test, R. Taherian et al. [56] applied voltage difference by connecting the sample to a power source. The power was kept constant (5, 8, 12, 15W) by adjusting the voltage and amperage. It's known that power is directly proportional to resistance and current square, as shown in equation 2.6.

$$P = I^2R \quad (2.6)$$

Where:

$P$  = Power, measured in watts (W)

$I$  = Current, measured in ampere (A)

$R$  = Resistance, measured in ohms ( $\Omega$ )

Since temperature increases through the sample's resistance, the ohmic resistance in equation 2.6 was controlled such that the induced power was assumed to be constant. During the joule heating test, samples' surface temperature was determined using a digital thermometer sensor. Details about this can be found in [56].

The setup of the joule heating test by [56] is shown in figure 2.11, while figure 2.12 describes the surface temperature variation with time at three constant applied voltages.

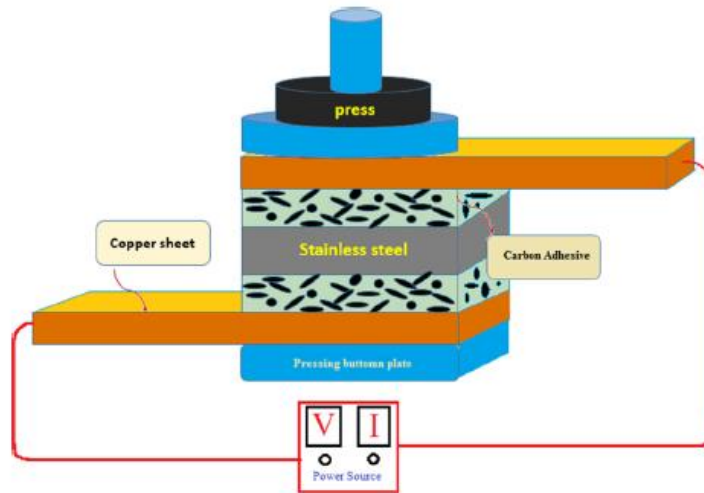


Fig. 2.11. Schematic of the setup for Joule heating testing [56]

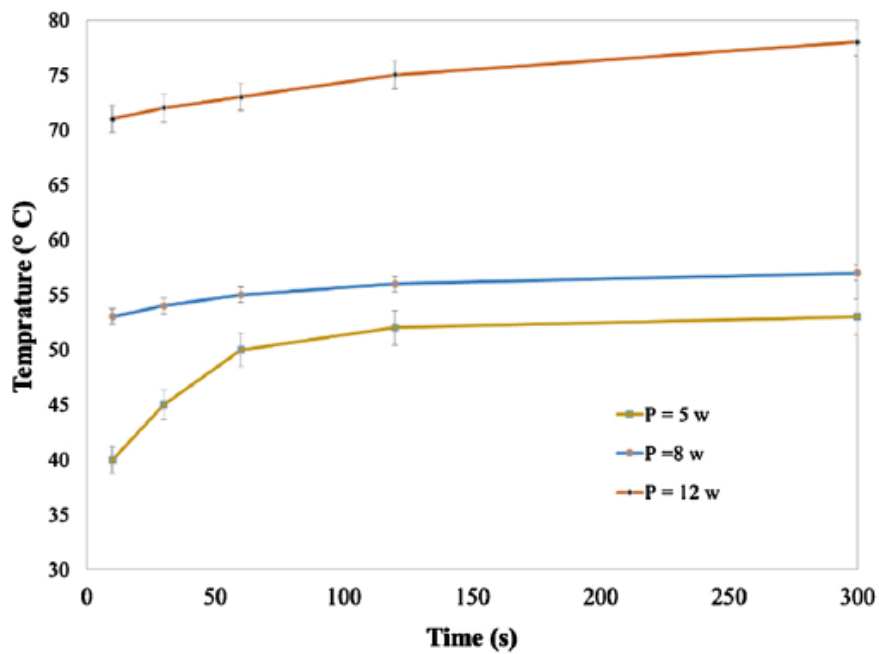


Fig. 2.12. Surface temperature evolution with power and time during joule heating [56]

Amongst the few works that analyzed the electro-thermal behavior of conductive polymeric composite, [2], [4], [5], [56] were one of the recent studies that used indirect heating. The composites were subjected to DC applied voltage till temperature and current stabilization was reached. Furthermore, an increase in temperature leading to a rise in internal resistance, and a reduction in conducted current, was observed. The heat generated is reduced over time until it equals the amount of heat dissipated by convection and radiation, resulting in thermal equilibrium. As a result, these CB-PLA materials could serve as a current limiter, restricting current consumption for some electric loads and introducing applications as safety devices.

#### **2.4.4 Stability Criteria**

These standards are needed to quantify the stabilization of the heated composite sample. The stability criterion is expressed in terms of current and temperature. The stability period grows with applied voltage.

The stabilization period depends on the voltage applied. Consideration is given to the influence of voltage on stabilization time for each printing orientation and its bilateral temperature/resistance dependence before, during, and after the glass transition (defined in section 2.2); this helps in analyzing the formation of a new conductive path through a process called sintering [2] and a probable destabilization due to high temperature.

### **2.5 Summary**

In line with this review, this study to research and analyze the electrothermal properties of 3D CB-PLA conductive composite materials of several sample types, with three variations in printing orientations, dimensions, and heating with AC applied voltage, is a good choice. An in-depth study of the material's behavior when exposed to high AC electrical potential is important to make progress in the field of multifunctional conductive structures

The results of this work would contribute to ongoing research in composites material structures, giving experimental background for the degradation of devices and exploring their future applications and operating limits.

# CHAPTER 3

## EXPERIMENTAL PROCEDURE

### 3.1 Preamble

This work relied on the state-of-the-art of Joule heating effect for the formulation of several parts of the work, the experimental setup, and results from the computation.

### 3.2 Experimental targets

This experiment is targeted toward achieving the following:

1. To investigate the electro-thermal interplay of the conductive composite of Polylactic acid with carbon black fillers (CB-PLA).
2. To obtain the electro-thermal response of CB-PLA under AC applied voltage. Unlike previous research, which applied DC constant voltage.
3. To analyze the influence of printing orientation and length on this interplay.
4. To monitor samples' temperature field, current, and resistance evolution over time.
5. To monitor stability with respect to the applied voltage.

### 3.3 Sample description

Based on the requirements, to study the electro-thermal behavior of conductive polymer of polylactic acid with carbon black fillers (CB-PLA), AC voltage was applied to the samples. Majorly, nine conditions were considered using rectangular composite samples; this account for three 3D printing orientations, with each orientation having three different lengths. The printing orientation includes transverse, oblique, and longitudinal. For the 3D manufacturing process, building on the previous work of [2], who used thin rectangular samples to mitigate premature failure in 3D printed samples as a result of stress concentration at the radius of the fillet. This provided great mechanical behavior when performing tensile tests. This choice of simple geometry contributed to the ease of imposing and analyzing electrical behaviour. To create a pattern in the sample, the

filaments were deposited in the specimen matrix. Additionally, three filament directions were created to allow for oblique ( $\pm 45^\circ$ ), longitudinal ( $0^\circ$ ), and transverse ( $90^\circ$ ) printing orientations. The following printing parameters were utilized to produce the samples; layer height of 0.2 mm, an air gap of 0 mm, road width of 0.4 mm, printing temperature of 230 °C, build plate temperature of 60 °C, infill density of 100%, printing speed of 30 mm/s, and a contour deposition along the component edge [2].

The sample dimensions (1L, 2L, 2.75L) considered in this present study are listed in Table 3.1.

TABLE 3.1. TEST SAMPLES DIMENSIONS AND PRINTING ORIENTATIONS.

Printing Orientation	Dimension		
	1L	2L	2.75L
Transverse ( $90^\circ$ )	82.5×13×3mm	165×13×3mm	240×13×3mm
Oblique ( $\pm 45^\circ$ )	82.5×13×3mm	165×13×3mm	240×13×3mm
Longitudinal ( $0^\circ$ )	82.5×13×3mm	165×13×3mm	240×13×3mm

Owing to the dielectric property of the polymeric matrix of PLA, the microstructure arrangement of carbon black within the polymeric matrix defines the nature of the conductive behavior of 3D printed conductive composites (CB-PLA) and the electric paths. These electric paths were formed at two levels: the filament level, which provided electric conduction in the direction of the filament, and the interfilament level, which provided electric conduction between various filaments. The effectiveness of the conductive composite and the impact of the printing direction is thus determined by these characteristics and the variations in the development of electric channels within and between filaments. For further analysis of the microstructural characterization of these specimens, a scanning electron microscope (SEM) was used, and images were captured. Detailed information on this procedure is found in section 2.3. of [2].

### 3.4 Experimental Setup

The experimental setup has the following main elements to describe.

1. Power supply unit
2. Measuring units
3. Software and data analysis

#### 3.4.1 Power supply unit

A variac AC power supply source (Verilec model, type arc-4-2) was used. It is a heavy unit with high maximum power output (0-250V @ 50Hz). It has an analog display to monitor the potential and output where multimeter or loads can be connected.



(a)



(b)



(c)

Fig. 3.1. Verilec AC power source, type arc-4-2. (a) the front view. (b) top view. (c) back view.

### 3.4.2 Measuring Units

Three variables were measured during the test these are the maximum temperature ( $T_{max}$ ), current ( $I$ ), average temperature ( $T_{avg}$ ), and applied AC voltages. The measurement of the applied voltage was also necessary since the disconnection of one of the samples provoked a small change in the voltage supplied to other connected samples.

### Multimeter

In the literature device, the multimeter is a measurement device for measuring multiple electrical parameters. It's capable of both DC and AC measurement. It can be used to take resistance, voltage, and current readings either as an ohmmeter, voltmeter, or ammeter, respectively. In this work, three ammeters were used to measure the current flowing through the three samples subjected to the same voltage.



Fig. 3.2. Digital Multimeter.

## **Infrared (IR) Camera**

The Fluke Ti50FT-20 IR model is an IR FlexCam thermal imager that outputs quality images. It is a battery-powered infrared camera that can be used to capture and monitor the temperature field of an object. This IR camera is suitable for monitoring the sample's temperature evolution. It's a professional's choice when the highest sensitivity is required. They feature about 320 x 240 detectors with industry-leading thermal sensitivity of 0.05°C NETD (Noise Equivalent Temperature Difference) for high resolution and ultra-high-quality images.

In addition, with a frequency of 60Hz detector acquisition rate, temperatures are displayed in real-time on the large 5-inch color display [66], giving updated values of the maximum temperature detected by the lens. It possesses features of IR-Fusion™ [66] technology, which captures a visible light image in addition to the infrared image; this helps IR image analysis and focus the picture before taking a photograph. It also helps to uncover anomalies as well. The IR camera has storage to save the captured thermal images, which are then transferred to the software (Fluke Connect) on a desktop to obtain several additional parameters, such as the average temperature ( $T_{avg}$ ). Figure 3.3 gives a pictorial view of the Fluke Ti50FT-20 IR camera. (a) full kit. (b) screen.



Fig. 3.3. Fluke Ti50FT-20 IR camera. (a) full kit. (b) screen

### 3.4.2 Software and data analysis

The software (Fluke Connect) was used to obtain the samples' average temperature ( $T_{avg}$ ), while MATLAB and Microsoft Excel were used for the data computation and analysis; this involves making tables, plotting graphs, and making comparisons

#### Fluke Connect

Using the Fluke Connect, the samples' average temperature ( $T_{avg}$ ) was obtained from the captured thermal images of samples/conductive composites. It is a key interface for downloading thermal imaging measurements, creating thermal reports and has room for cloud synchronization. Fluke Connect has both mobile, web, and desktop apps. A polygon was drawn around the edges of each thermal image to obtain the  $T_{avg}$  (average temperature) from the thermal images, as shown in figure 3.4. The polygon was drawn such that the overall temperature dispersion on each filament's sample (which is the area of interest) was captured. The maximum, average, and minimum temperatures were displayed, and the average temperature was obtained, as shown in figure 3.4.

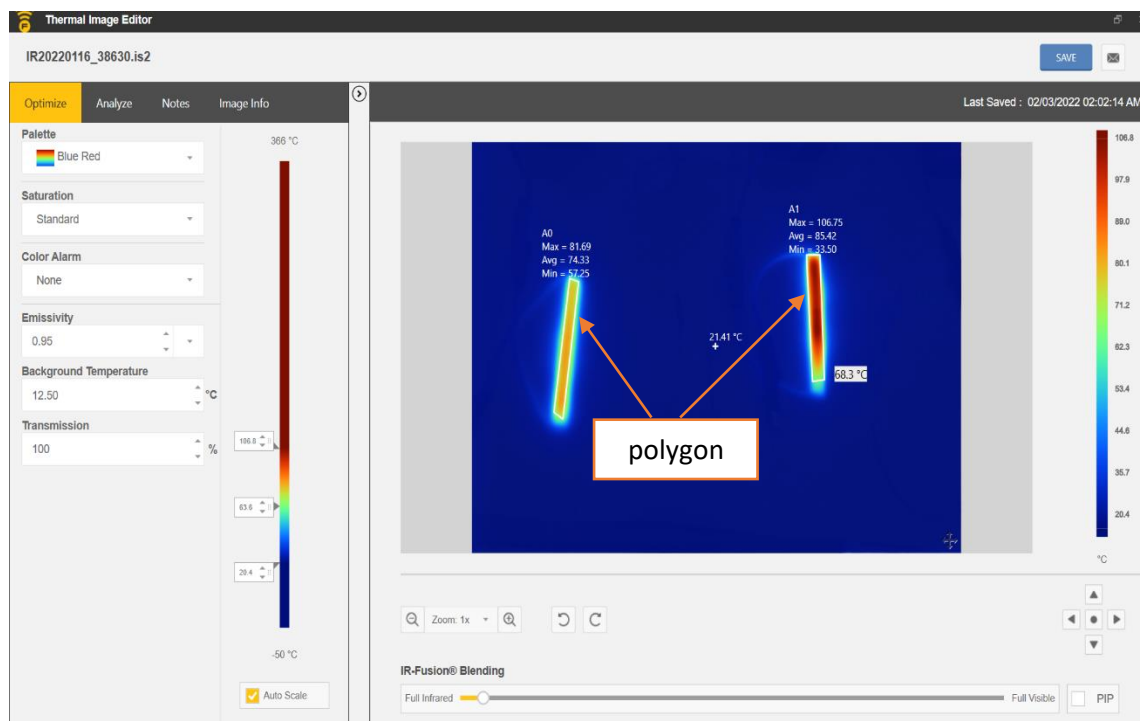


Fig 3.4. Derivation of samples' average temperature from the analysis of thermal images using Fluke Connect.

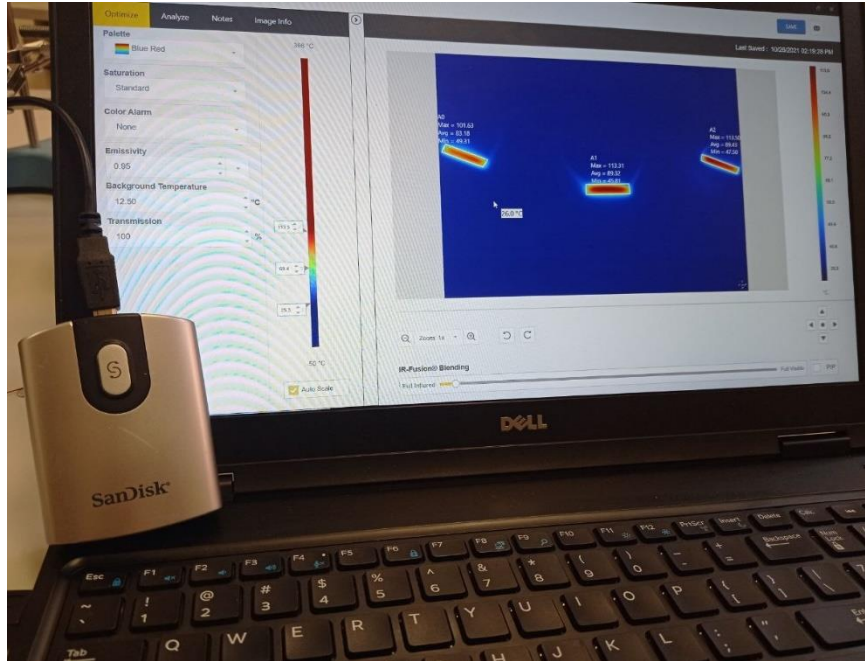


Fig. 3.5. SanDisk card reader connected to the laptop to analyze thermal images on Fluke Connect.

## 3.5 Experimental Procedure

### 3.5.1 Composite heating and heating schedules

Each series of the test starts with AC voltage applied at an initial time  $t_0$  equals zero-minute, readings were taken every 5 minutes till current and temperature stability were reached (stability analysis is described in 3.3 b.). Once stabilization is reached, the applied voltage is turned off, and the samples are allowed to cool to room temperature before repeating the same process with an increased supply of AC voltage. Here, the assignment of the test was to apply the same value of AC voltage to three samples of the same length but with different printing orientations at the same time instant. For example, supplying 30 volts to a 1L, 2L, and 2.75L. To optimize the study, three variables were measured at every 5 minutes interval these are the maximum sample temperature ( $T_{max}$ ), current and average sample temperature ( $T_{avg}$ ). The maximum temperature and current were obtained directly during the test. The thermal pictures of the samples were taken using a Fluke IR camera every 5 minutes during the test till stabilization and then analyzed using Fluke connect software on the desktop to obtain the average temperature ( $T_{avg}$ ).

For 1L samples, the voltage range used was 25V to 45V; for 2L samples, it was 25V to 80V, and for 2.75L, it was 30V to 120V. These ranges were selected to achieve equal heating in the samples regardless of their length.

The voltage steps for each sample are shown in table 3.2.

TABLE 3.2. EXPERIMENTAL STEPS OF AC VOLTAGES IMPOSED ON COMPOSITE SAMPLES

Composite Samples (Varying length)	Applied AC Voltages (Volts)								
	1L	25	30	40	45				
2L	30	40	50	60	70	80			
2.75L	40	50	60	70	80	90	100	110	120

### 3.5.2 Stability Analysis

Applied AC voltage is imposed on the samples till current and temperature stabilization are obtained. To obtain stabilization, the difference between two maximum temperature values and two current values (i.e., between consecutive measurements) at  $t_n$  and  $t_N$  are observed (with n increasing in the step of 5 for 1L samples and by 10 for 2L and 2.75L samples). To declare a sample stable during the test, then:

$$T_{max t_{n+5}} - T_{max t_n} < 0.5^{\circ}C \quad (3.1)$$

$$I_{t_n} - I_{t_{n+5}} < 1mA \quad (3.2)$$

$T_{max t_n}$  = Maximum temperature at an instant time, measured in degree Celsius.

$I_{t_n}$  = Consumed current at  $t_n$ , measured in milliampere.  $n = 0, 5, 10, \dots, N$ .

The data obtained were then analyzed, and graphs were plotted using MATLAB, which is a mathematical analysis software, and Microsoft Excel. The experimental test can be summarized with the flow chart in Figure 3.6.

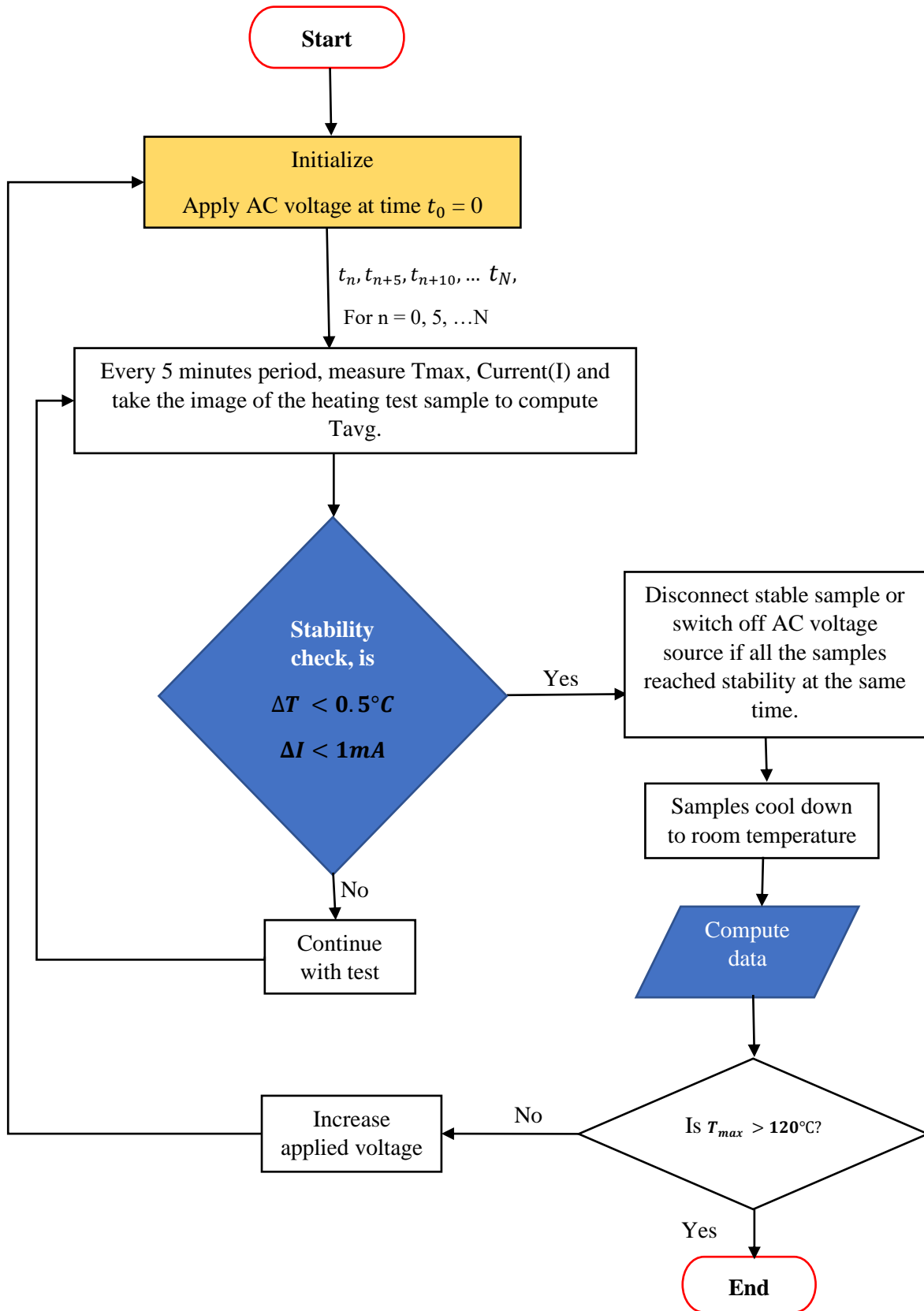


Fig. 3.6. Flow chart of the electro-thermal experimental test.

Figure 3.7 shows the experimental setup used to study the electro-thermal interplay of conductive composites of polylactic acid with carbon black fillers using AC applied voltage.

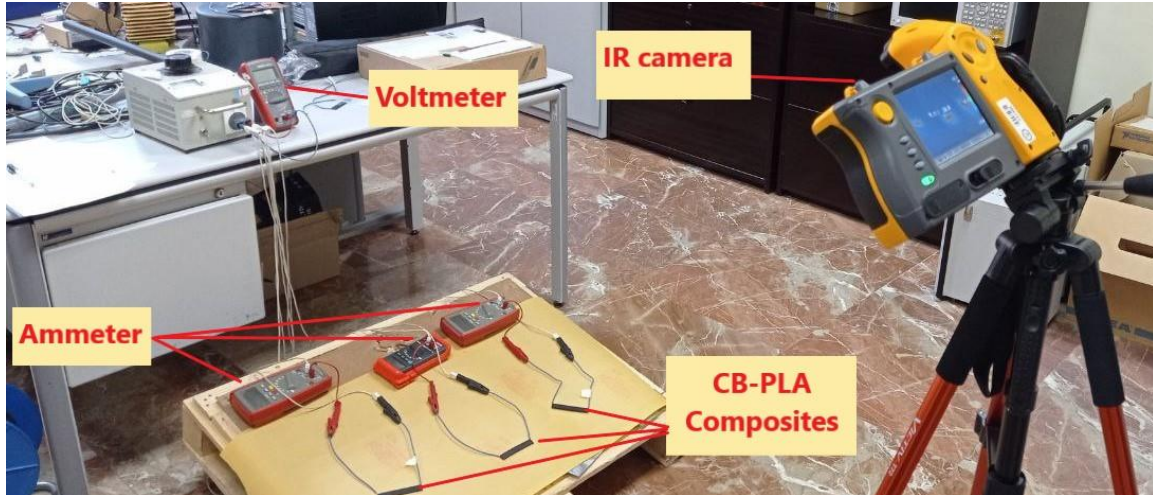


Fig. 3.7. Electro-thermal test for CB-PLA setup

The equivalent circuit of the composite samples' connection to the AC voltage source, voltmeter, and Ammeter is shown in Figure 3.8

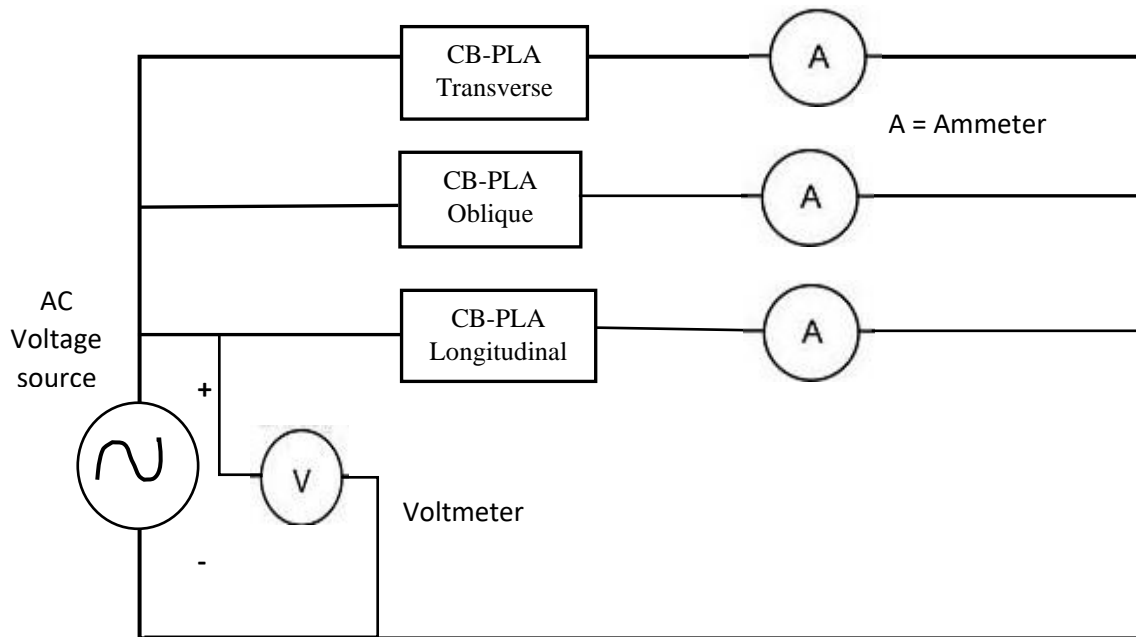


Fig. 3.8. Equivalent circuit of the electro-thermal test setup for CB-PLA.

## CHAPTER 4

### RESULTS AND DISCUSSION

During the experiment, resistance, temperature, and current values were measured and analyzed using analytical tools such as Microsoft Excel, MATLAB, and Fluke Connect. Values of the maximum temperature ( $T_{max}$ ), AC current ( $I_{mA}$ ), resistance ( $R$ ), and voltage ( $V$ ) were obtained in real-time during the experimental activity, while the average temperature was obtained using Fluke Connect (a thermal image analytical tool). The process of obtaining the average temperature ( $T_{avg}$ ) from the thermal images was discussed earlier in chapter 3.

Subjecting the samples to AC voltage, heat is generated, leading to temperature increment due to the resistive behaviour of the material. In addition, it is expected a bilateral coupling which promotes an increase in internal resistance and subsequent current reduction due to temperature increment, according to previous work [2]. Current reduction further reduces the heat dissipated till thermal and electrical equilibrium is obtained. This behaviour obeys Joule's effect, which was described by equation (2.1) in chapter 2.

For clarity on the characterization of the electro-thermal response of Poly lactic acid filled with carbon black particles (CB-PLA), the following results have been analyzed and discussed in this chapter.

1. Resistive and thermal response of tested CB-PLA
2. Geometry contribution – contribution of varying length.

A total of nine conditions were considered according to the printing orientations (Transverse, Oblique, and Longitudinal) and sample geometrical length (1L, 2L, 2.75L), i.e., sample length was varied while other dimensions were kept constant.

#### 4.1 1L Samples

Three 1L samples of transverse, oblique, and longitudinal printing orientations were subjected to AC applied voltages 25V, 30V, 40V, and 45V. Voltage increment was introduced for further test after thermal and current stabilization had been achieved and

stopped for a sample where destabilization arose till the three samples were destabilized. For this sample, destabilization occurred at an applied voltage of 45V. To go further, let us evaluate the samples' overall behaviour.

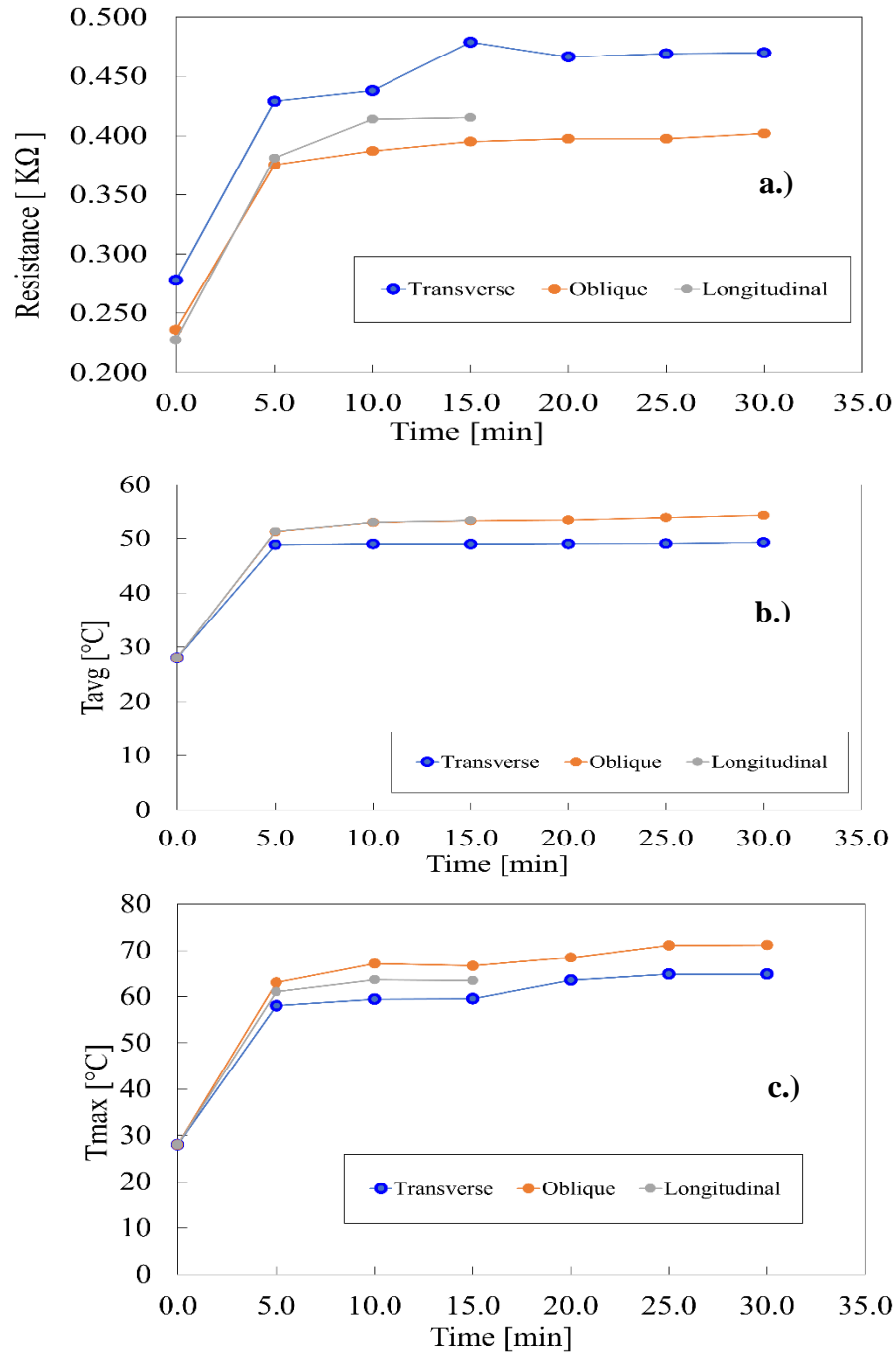


Fig. 4.1. Experimental results for IL samples heated by Joule effect imposing AC voltage 25V. These results are presented for transverse, oblique, and longitudinal samples. a.) Electric resistance is plotted against time. b.) Average temperature is plotted against time. c.) Maximum temperature is plotted against time.

From figure 4.1, at an applied voltage of 25V, the longitudinal sample got into equilibrium early (at 15 minutes); this is due to its low resistance value (0.415  $\Omega$ ). This could be explained by composites' behaviour, exhibiting the highest temperature value and least resistance value. This result is explained by the direct relationship between heat generated via Joule's effect and sample resistance, as described in equation 2.1. Ideally, the resistance and temperature values of the oblique sample ( $\pm 90^\circ$ ) were expected to be in-between that of transverse and longitudinal samples or close to the resistance value of the longitudinal sample. This is explained by the nature of its conductive path when compared to longitudinal ( $0^\circ$ ) and transverse samples ( $+90^\circ$ ). This is attributed to the electric current pathways in the filaments. In longitudinal samples, electric current flows directly through the filaments, while in oblique samples, it flows through the interfilament path. The interfilament path's angular deviation is more in transverse samples. However, the test results show that at a low applied voltage in the 1L sample, the resistance value of the oblique sample goes below the resistance value of the longitudinal sample. This response from the oblique sample 1L could be due to the presence of voids or errors during the printing operation.

Table A.1 in the appendix also shows the current, temperature, and resistance evolution of the three samples.

Studying the current and temperature evolution from table 4.1, current decreases with time while temperature increases with time till saturation. Samples resistance values also increased with temperature. However, the sample with the highest resistance value had the lowest temperature value, which is expected by equation (2.1). In this case, the transverse sample presented the lowest temperature value and highest resistance value, a behaviour that could be explained by the contribution of the interfilament pattern and possible sintering process.

At 30V, as could be seen in figure 4.2, the behaviour of 1L samples is similar to the result at 25V. However, beyond 30V (i.e., from 40 V to 45V imposed AC voltages), a significant change in resistance trend at thermal equilibrium was detected; this could be the effect of possible sample degradation from previous and present tests.

## Summary:

- The growth in resistance with temperature is confirmed for AC voltage.
- The larger the applied voltage, the longer the stabilization time (if reached), which is expected from equation (2.1).
- The transverse sample shows the lowest temperature and current value but the highest resistance value.
- Specimen with the highest temperature value shows the lowest resistance value and highest current value. In the 1L sample, this behaviour occurred in the oblique instead of in the longitudinal sample. Also, the oblique sample showed the highest current value.
- This result of the 1L oblique sample at several applied AC voltage values shows an indication of likely printing error during the printing process.
- The longitudinal sample got destabilized at 40V, whereas oblique and transverse samples required higher voltages (45V).
- Transverse and oblique samples got destabilized at 45V and at high temperatures.

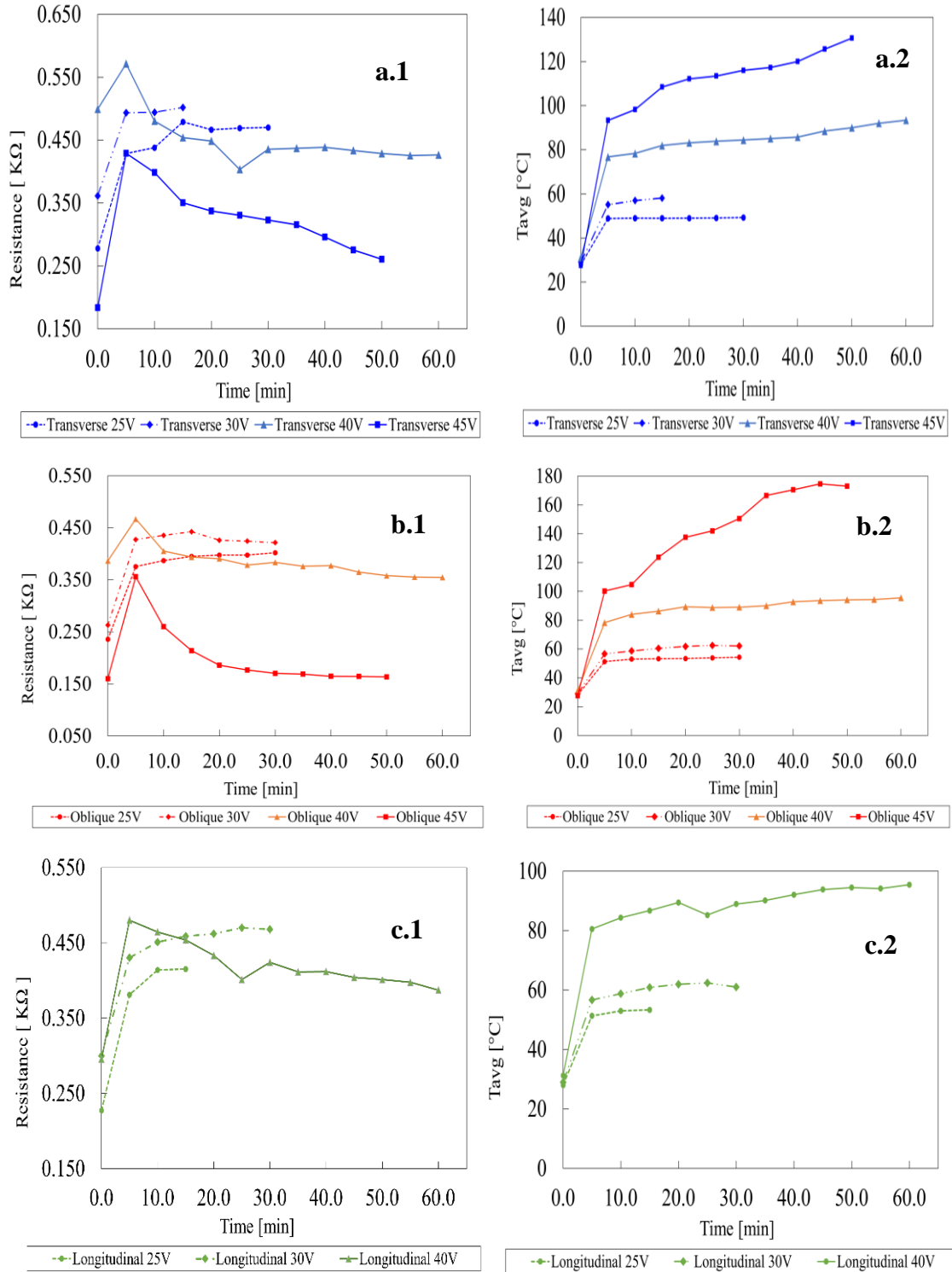


Fig. 4.2. Experimental temperature and resistance results for 1L samples heated by Joule effect, imposing AC voltages from 25V to 45V. a. transverse sample, b. oblique sample and c. longitudinal sample.

## 4.2 2L Samples

These samples comprise three printing orientations which are transverse, longitudinal, and oblique, but with a X2 length factor of 1L as described in section 3.3 of chapter 3. These samples were subjected to AC voltages - 30V, 40V, 50V, 60V, 70V, and 80V.

As shown in figure 4.3, the transverse sample showed the least temperature again, highest resistance, and least current values compared to oblique and longitudinal samples during the heating process. This result is a contribution of filament orientation.

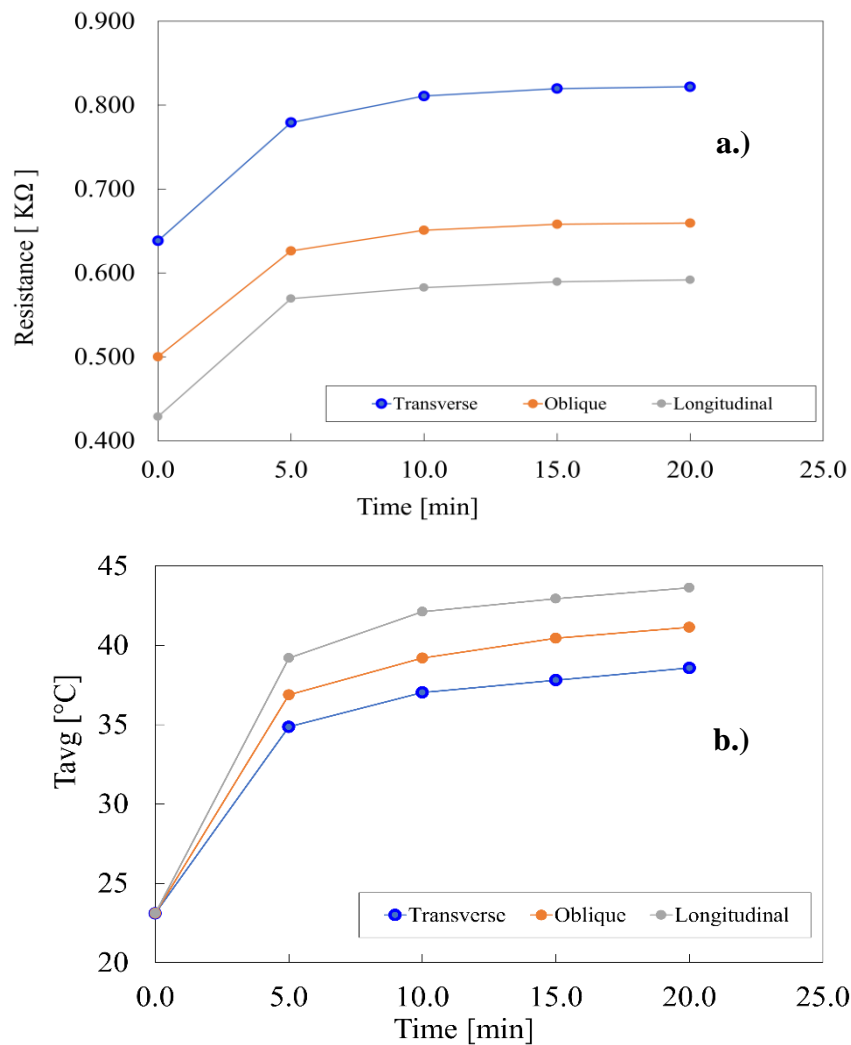


Fig. 4.3. Experimental resistance and temperature results for 2L samples subjected to AC voltage 30V. These results are presented for transverse, oblique, and longitudinal samples. a.) Electric resistance is plotted against time. b.) Average temperature is plotted against time.

From Figures 4.3 and 4.4, it could be seen that the longitudinal sample exhibits the least resistance value and highest temperature. This behaviour of the longitudinal sample in 2L is influenced by the alignment of the filaments' conductive path (during printing) with the electrodes used to supply AC voltage to the composite material (CB-PLA). The electrodes were positioned such that current flows along the longitudinal axis. This arrangement improves the overall electric response of the longitudinal sample, reducing the contribution and presence of voids along the filament. Furthermore, just like in the 1L sample, the longitudinal sample was destabilized first at 70V due to low resistance value characteristics, while transverse and oblique samples got into disequilibrium at 80V.

Again, just as in 1L samples, beyond 60V imposed AC voltage for 2L, a significant change in resistance trend after thermal equilibrium was detected for all printing directions with applied voltage, which could be a contribution of possible sample degradation from previous tests (temperature effect). This is seen in figure 4.4.

The results of 2L samples were compared to that of 1L samples, using figures 4.1, 4.2, 4.3, and 4.4; one remarkable observation was that the longitudinal sample in 2L showed the least resistance values and highest temperature value. This was different from what was observed earlier in 1L samples, where the oblique sample presented this characteristic.

In this chapter, the comparison of 1L with 2L samples is properly discussed for quantitative study of the linear properties of the material. The graphs of resistance vs. time, and temperature against time, superimposing 25V (for L samples) and 50 V (for 2L samples) curves were shown. Also, that of 30V/1L was compared with 60V/2L. Comparison with 2.75L samples will not be quite accurate since the voltage levels do not follow the x2.75 factor, except for 40V (L) and 110V (2.75L; which was quite high, leading to instability).

**Summary:**

- The growth in resistance with temperature is confirmed for AC voltage.
- The larger the applied voltage, the longer the stabilization time (if reached), which is expected from equation (2.1).
- The transverse sample shows the least temperature and current value but the highest resistance value.
- Specimen with the highest temperature value shows the lowest resistance value and highest current value. This behaviour was exhibited by the longitudinal sample
- The longitudinal sample got destabilized at 70V, whereas oblique and transverse samples required higher voltages (80V).
- Transverse and oblique samples got destabilized at 80V and at high temperatures.

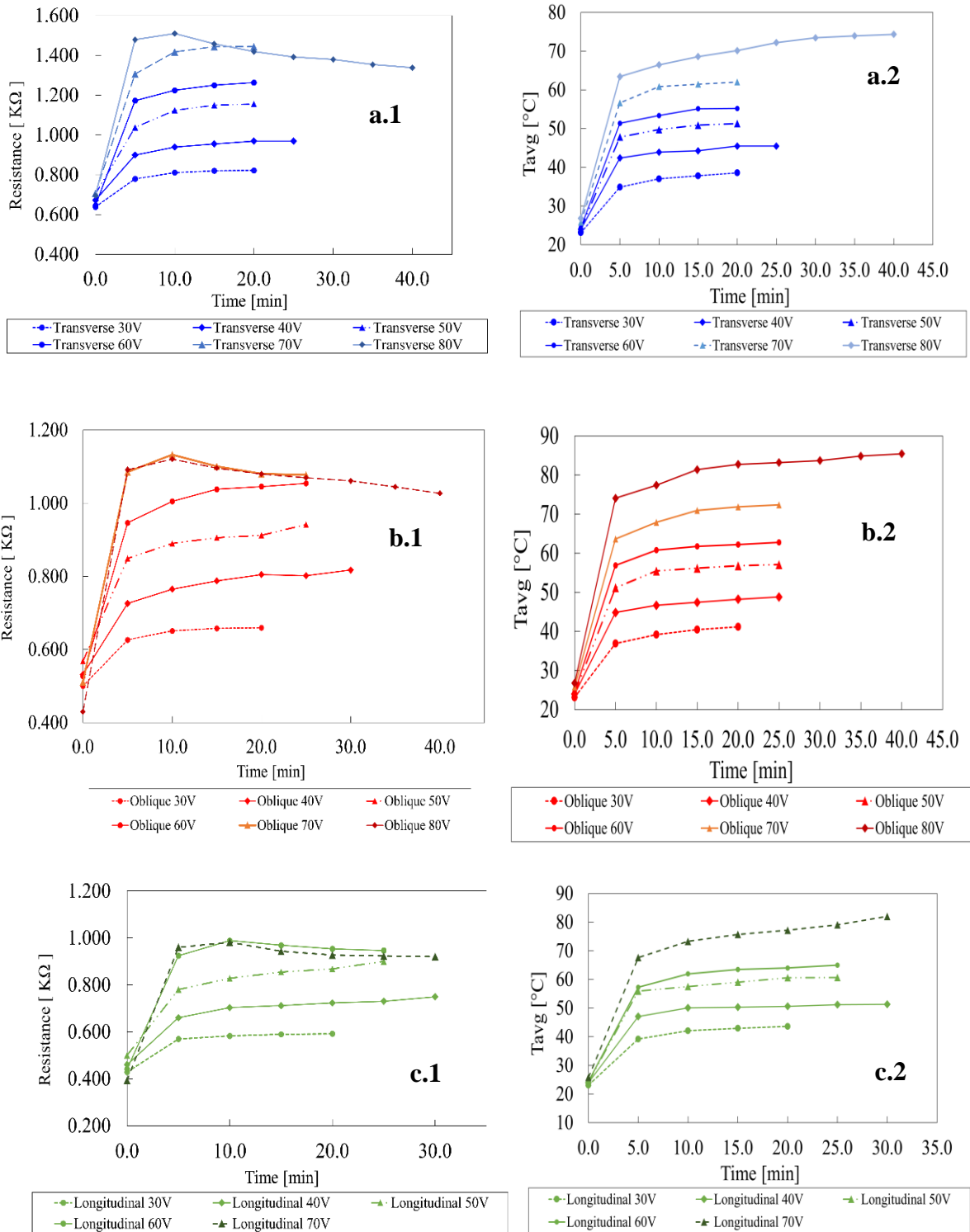


Fig. 4.4. Experimental temperature and resistance results for 2L samples heated by Joule effect, imposing AC voltages from 30V to 80V. a. transverse sample, b. oblique sample and c. longitudinal sample.

### 4.3 2.75L Samples

The samples were subjected to several voltage values following the same experimental procedure as that of 1L and 2L samples, which were heated by the Joule effect. The samples were subjected to AC voltages – 30V, 40V, 50V, 60V, 70V, 80V, 90V, 100V, 110V, and 120V. Figure 4.5 shows the experimental resistance and temperature results when the 2.75L sample was subjected to 30V AC voltage.

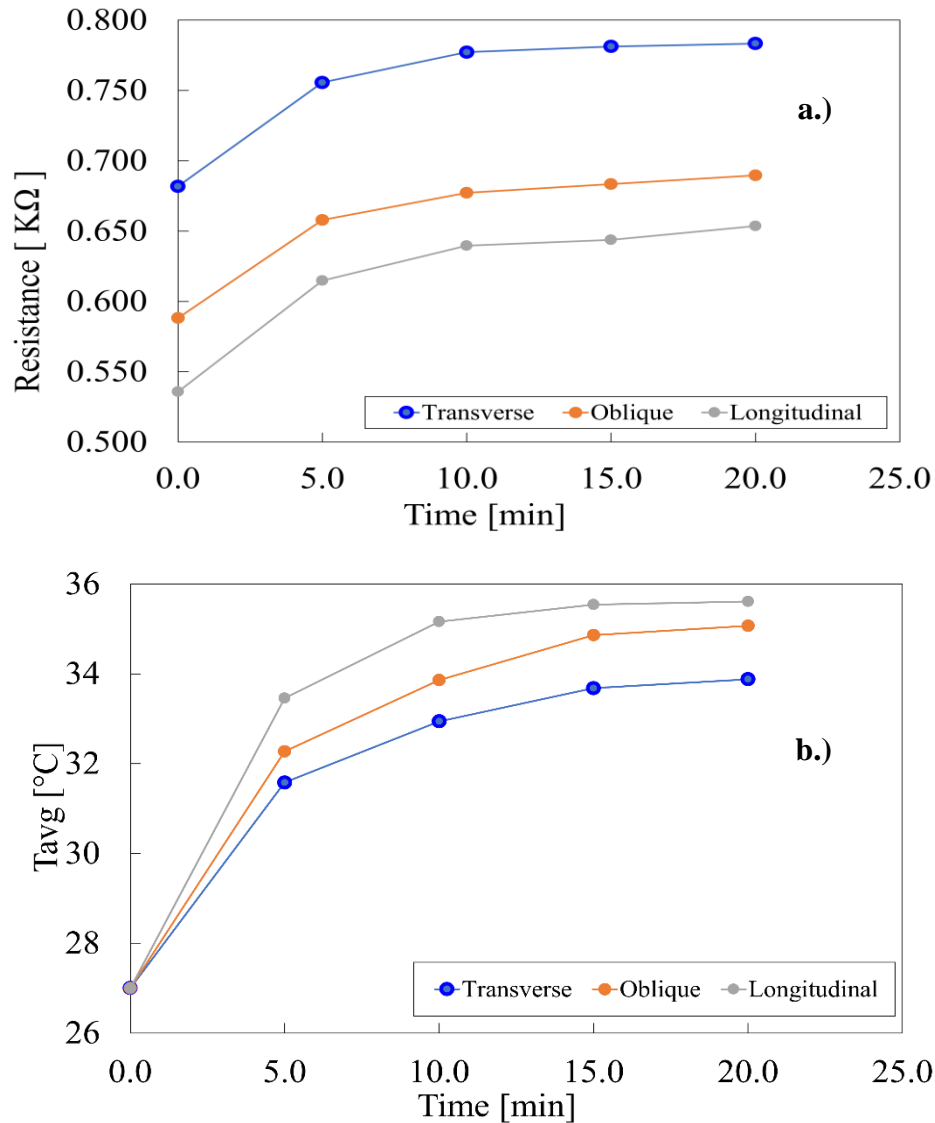


Fig. 4.5. Experimental resistance and temperature results for 2.75L samples subjected to AC voltage 30V. These results are presented for transverse, oblique, and longitudinal samples. a.) Electric resistance is plotted against time. b.) Average temperature is plotted against time.

As observed in previous cases, in figure 4.5, the transverse sample shows the largest resistance values during all heating processes, leading to the lowest temperature value (according to Joule effect). In figure 4.6 below, significant growth in resistance values after equilibrium was observed for all printing directions with applied voltage. This could be a contribution of possible sample degradation from previous test.

A consistent observation in the results of 2.75L in figure 4.6 when compared with previous length samples (1L and 2L), the longitudinal sample got out of equilibrium first, as expected, since it has the least resistance. This response is due to its minimum resistance value compared to transverse and oblique samples. Although, it was hypothesized to have transverse and oblique samples out of equilibrium at 110 V applied AC voltage. However, the transverse sample obeyed the stability criterion at 110V and got destabilized at 120V.

**Summary:**

- The growth in resistance with temperature is confirmed for AC voltage.
- The larger the applied voltage, the longer the stabilization time (if reached), which is expected from equation (2.1).
- The transverse sample shows the lowest temperature and current value but the highest resistance value.
- The longitudinal specimen shows the highest temperature value, least resistance, and highest current value.
- The longitudinal sample got destabilized at 100V, whereas oblique and transverse samples required higher voltages.
- Transverse got destabilized at 120V and at high temperatures.
- Oblique samples got destabilized at 110V.

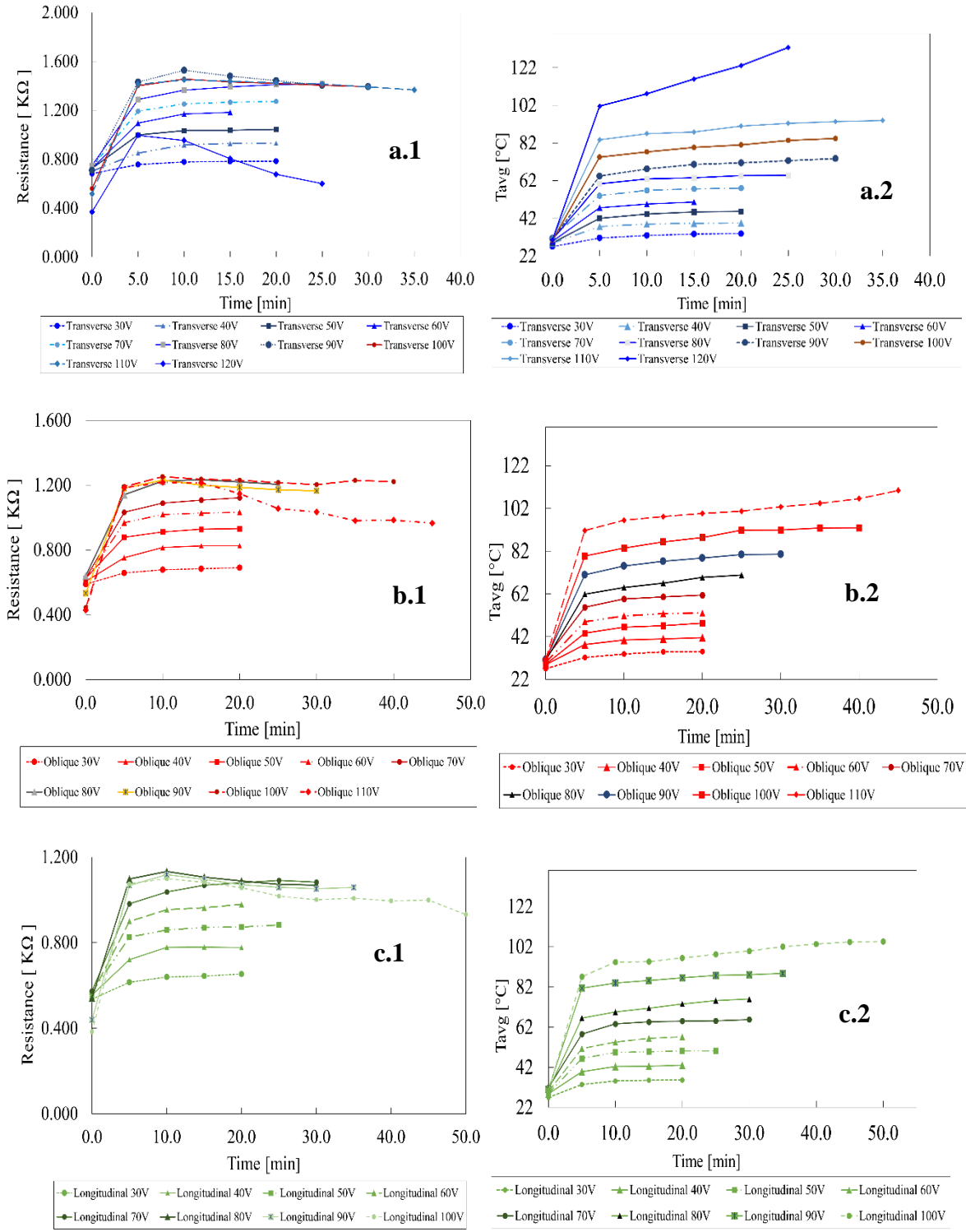


Fig. 4.6. Experimental temperature and resistance results for 2.75L samples heated by Joule effect, imposing AC voltages from 30V to 120V. a. transverse sample, b. oblique sample and c. longitudinal sample.

The overview of the experimental results of each sample type has been discussed. To further explain the electro thermal interplay, the following data analysis are further discussed in subsequent pages.

1. Resistive and thermal response of tested CB-PLA
2. Geometry contribution – contribution of varying length.

#### **4.4 Resistive and thermoelectric response of tested CB-PLA**

As seen in figures 4.1, 4.2, 4.3, 4.4, 4.5, 4.6, and 4.7, the largest change in temperature and current values in a step time occurred at the transition from 0 to 5 mins, which is the first 5 minutes of the experiment.

As seen in figure 4.7, which shows the plot of resistance against average temperature for 30V/1L, 60V/2L, and 90V/2.75L samples. There exists an evolution such that as the temperature increases due to current flow, the resistance value also increases till saturation, after which the resistance begins to decrease while the average temperature keeps increasing. This is well represented in 90V/2.75L. With respect to Figures 4.2, 4.4, and 4.6, this evolution continues till electrical and thermal equilibrium are reached, balancing the internal heating with convectional cooling. From figure 4.7, the plot of resistance against average time, it could be seen that the resistance increases linearly with the average temperature till the resistance reaches its peak value. Comparing the graph of 30V/1L with 60V/2L, it could be seen that doubling the length contributes to an approximate doubling of the resistance value but not the average temperature.

From the analysis of sample 2L using figure 4.8, the electric resistance increases as the temperature increases uniformly with time. The increase in sample resistance leads to a decrease in heat dissipated, according to equation 2.1 in chapter 2.

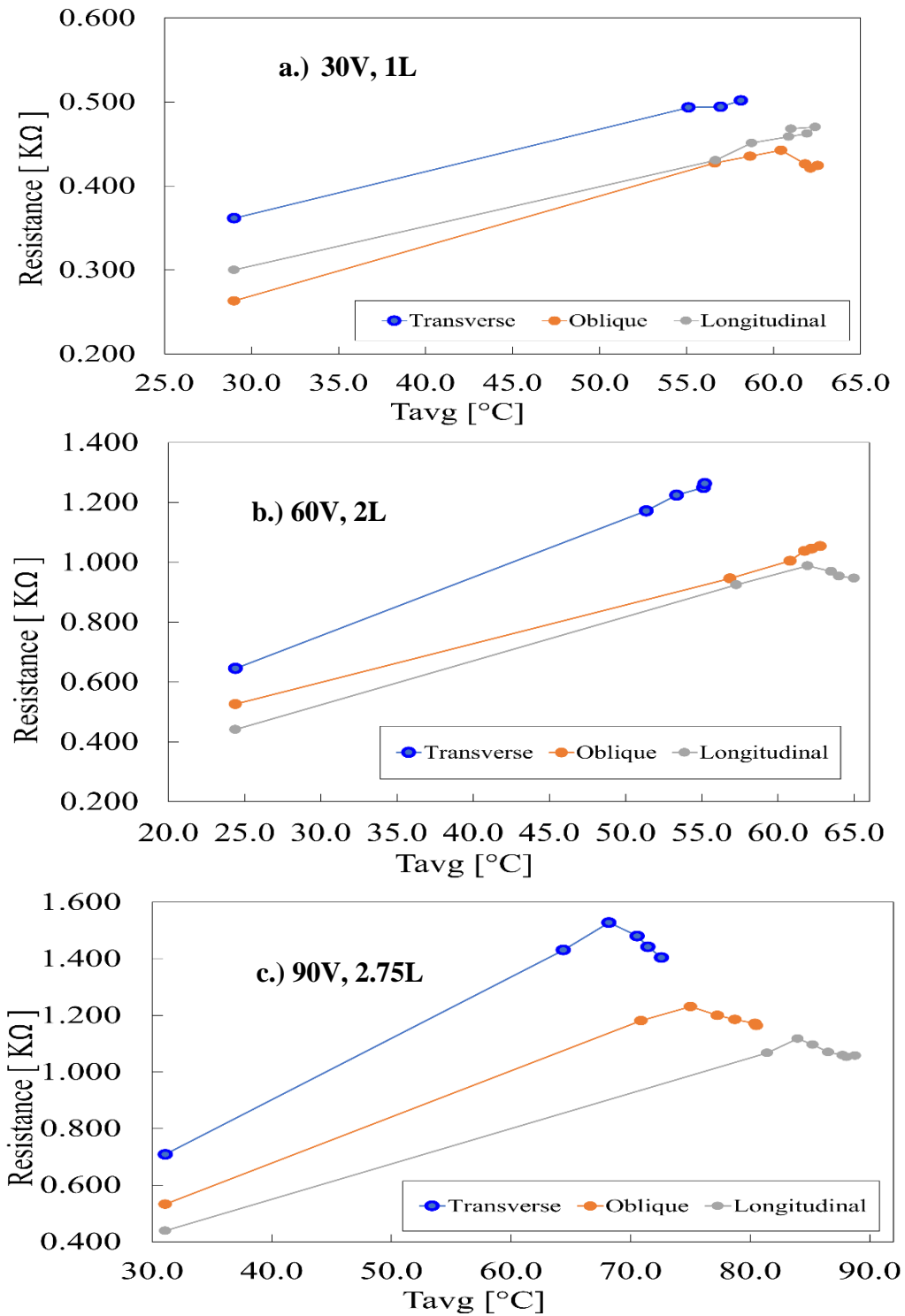


Fig. 4.7. Experimental resistance and temperature results for composite samples subjected to AC voltage. a.) Electric resistance is plotted against average temperature in 30V/1L sample. b.) Electric resistance is plotted against average temperature in 60V/2L sample. c.) Electric resistance is plotted against average temperature in 90V/2.75L sample.

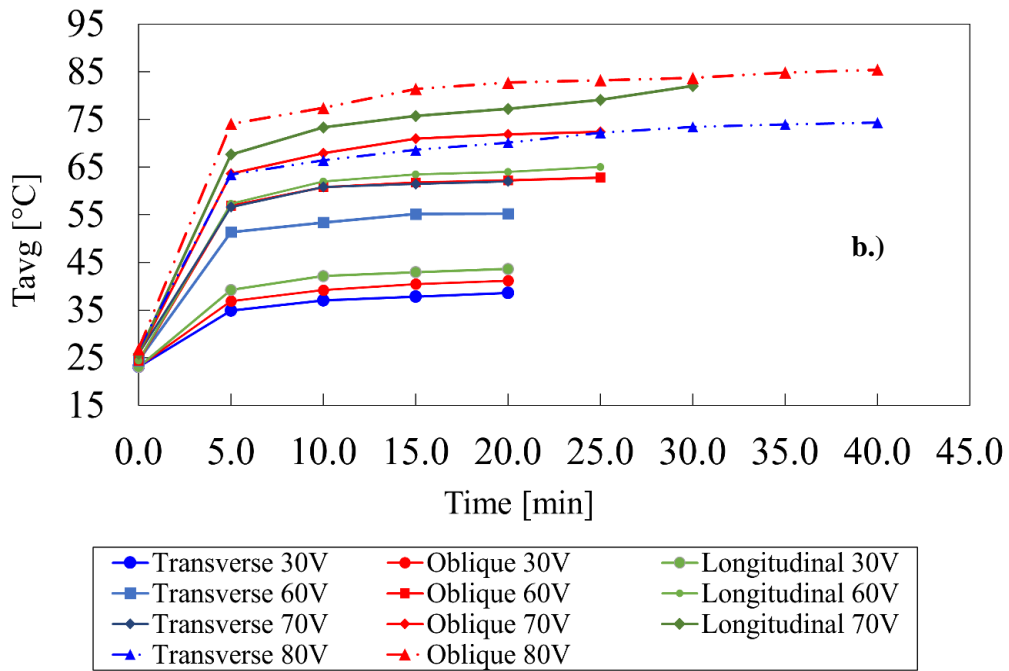
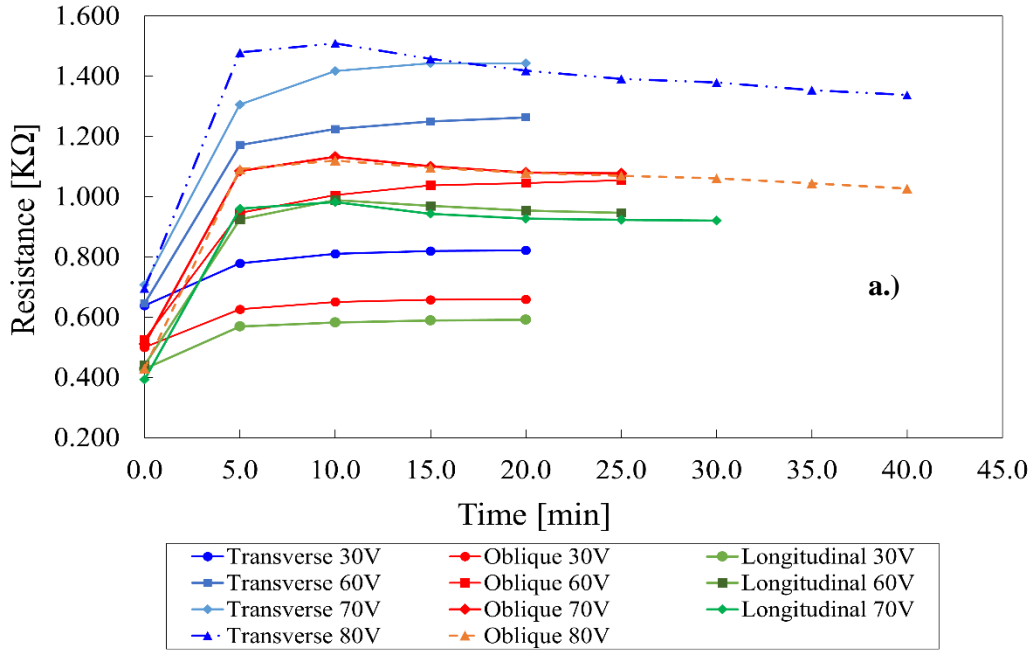


Fig. 4.8. Experimental resistance and temperature results for 2L samples subjected to AC voltage 30V to 80V. These results are presented for transverse, oblique, and longitudinal samples. a.) Electric resistance is plotted against time. b.) Average temperature is plotted against time.

#### 4.5 Stability and Stabilization Time

From figure 4.8, it was observed that sample stabilization was achieved in the three samples with all applied voltages from 30V to 80V except for voltages and samples where the heat rose to temperatures above 65 °C, thus getting the material into disequilibrium. At disequilibrium, the overall resistance of all samples begins to decrease while the temperature keeps rising rapidly. This is clearly illustrated by the dotted lines for transverse and oblique samples (also at 70V) and longitudinal samples (at 70V) in figure 4.8. Here transverse and oblique samples were at disequilibrium at 80V while the longitudinal sample was at disequilibrium at 70.

It's critical to understand the composite's glass transition response. The glass transition temperature of polylactic (PLA) matrix is estimated to be between 50 – 80 degrees Celsius. The instability observed could be due to this limit, which also seems to be confirmed by samples deformation observed (melting).

Illustrated in Figures 4.2, 4.4, and 4.6, below the glass transition, as the applied voltage heats up the samples, the temperature and resistance follow an increasing trend. This trend was observed below 30V for 1L, below 60V for 2L, and below 80V for 2.75L in longitudinal specimens. Beyond the glass transition point, the temperature keeps increasing while the resistance rises to its peak and then starts to fall till stabilization. This shows that exceeding the glass transition temperature of PLA composites changes the linear trend in its electro-thermal interplay.

From figures 4.1 – 4.8, the transverse sample is seen to have a response different from that of the longitudinal and oblique samples, with the latter samples having similar thermal and electric responses. This result obeys equation 2.1 from Joule effect, as the transverse sample shows the highest resistance value and obtained the lowest temperature compared to longitudinal and oblique samples; a typical example is found in the figures for 2L samples.

The stabilization time was evaluated with respect to the applied voltage and printing orientation. With reference to the result in figure 4.8, the stabilization time depends more on the applied voltage and not mainly on the printing orientations. Once the glass transition

voltage is exceeded, a further increment in applied voltage results in a decrease in stabilization time. This is seen in Figures 4.2 and 4.6 longitudinal samples, where the first voltage to reach the glass transition temperature (30V for 1L sample and 80V for 2.75L) takes longer to achieve stabilization, i.e., longer stabilization time. Although in the longitudinal 1L sample from figure 4.2, till the voltage at glass transition temperature was applied, the increase in stabilization time is an indication of increased applied AC voltage. This is seen in longitudinal sample 1L, 30V, which is the voltage to arrive at the glass transition temperature first. This claim is different from analyzing the 2L longitudinal sample, where 60V is the applied AC voltage that reached the glass transition temperature first. It could be seen from figure 4.4 that before glass transition temperature was reached, 40V applied voltage exhibits the longest stabilization time. In addition, for the 2.75L samples, 80V applied voltage was the first voltage to reach glass transition temperature ( $T_g$ ), exhibiting a longer stabilization time than other voltages below the glass transition voltage. The result of this interaction of applied AC voltage with stabilization time shows that below glass transition temperature voltage, an increase in voltage leads to an increase in stabilization time.

Overall, destabilization occurred at voltages that contribute to the increase in temperature till a high trigger temperature above 120 °C. This contribution also varies with sample types and length. For example, in 2.75L samples, the Oblique sample got destabilized at 120V compared to its counterparts, where the transverse sample destabilized at 110V and the longitudinal sample at 100V. However, in other sample lengths (1L and 2L), longitudinal and oblique samples exhibit similar behaviour, as seen in Figures 4.1 – 4.7. Also, one factor that appears to have a great influence on thermal stability is thermal inertia (property of a material that expresses the rate at which its temperature reaches the environmental temperature). Thermal inertia is simply described as a measure of a material's responsiveness to temperature variation.

Clearly, from figures 4.2, 4.4, and 4.6, the transverse sample shows the slowest thermal inertia, with this printing type not getting into destabilization before longitudinal and oblique samples. This slowness in destabilization in transverse samples shows the contribution to conduction through filaments and sintering process. This is an improvement

in polymeric chain mobility, resulting in electric conductivity at high temperatures and rearranging the conductive particles in the matrix.

#### **4.6 Influence of geometry on electrothermal response**

The dependence of the electrothermal response with composites length in 1L, 2L, and 2.75L samples was evaluated. From figure 4.9, temperature and resistance evolution for 25V/1L and 50V/2L were compared (representing the x2 factor). It is necessary to keep the ratio between applied voltage and length of the compared samples the same to evaluate the linearity. With reference to figure 4.9, it could be hypothesized that the electrothermal response of conductive composites (CB-PLA) is similar for all samples with the same factor (voltage to length ratio). Although increasing the length and voltage by a factor of  $\times 2$  almost doubles the resistance of each printing orientation, as seen in Table A.1 – A.4 from the appendix, figure 4.9, and figure 4.10, but the  $T_{avg}$  and  $T_{max}$  were not doubled.

In addition, from figure 4.10 and table A.1, A.2, the  $T_{avg}$  and  $T_{max}$  of each printing orientation of factor 1L gave values that were relatively close to the results obtained from samples of the same prints with a 2L factor when approaching equilibrium. Similar behaviour was observed in figure 4.1, where specimens of 30V/1L were compared with specimens of 60V/2L, and in appendices B and C, where specimens of 40V/1L were compared with 110V/2.75L. From the results, the linearity is not completely accomplished for resistance nor accomplished for average temperature ( $T_{avg}$ ) and maximum sample temperature ( $T_{max}$ ). In this regard, from the quantitative study of the composite materials' linear properties, it could be concluded that the overall electrothermal response of CB-PLA is independent of the sample length.

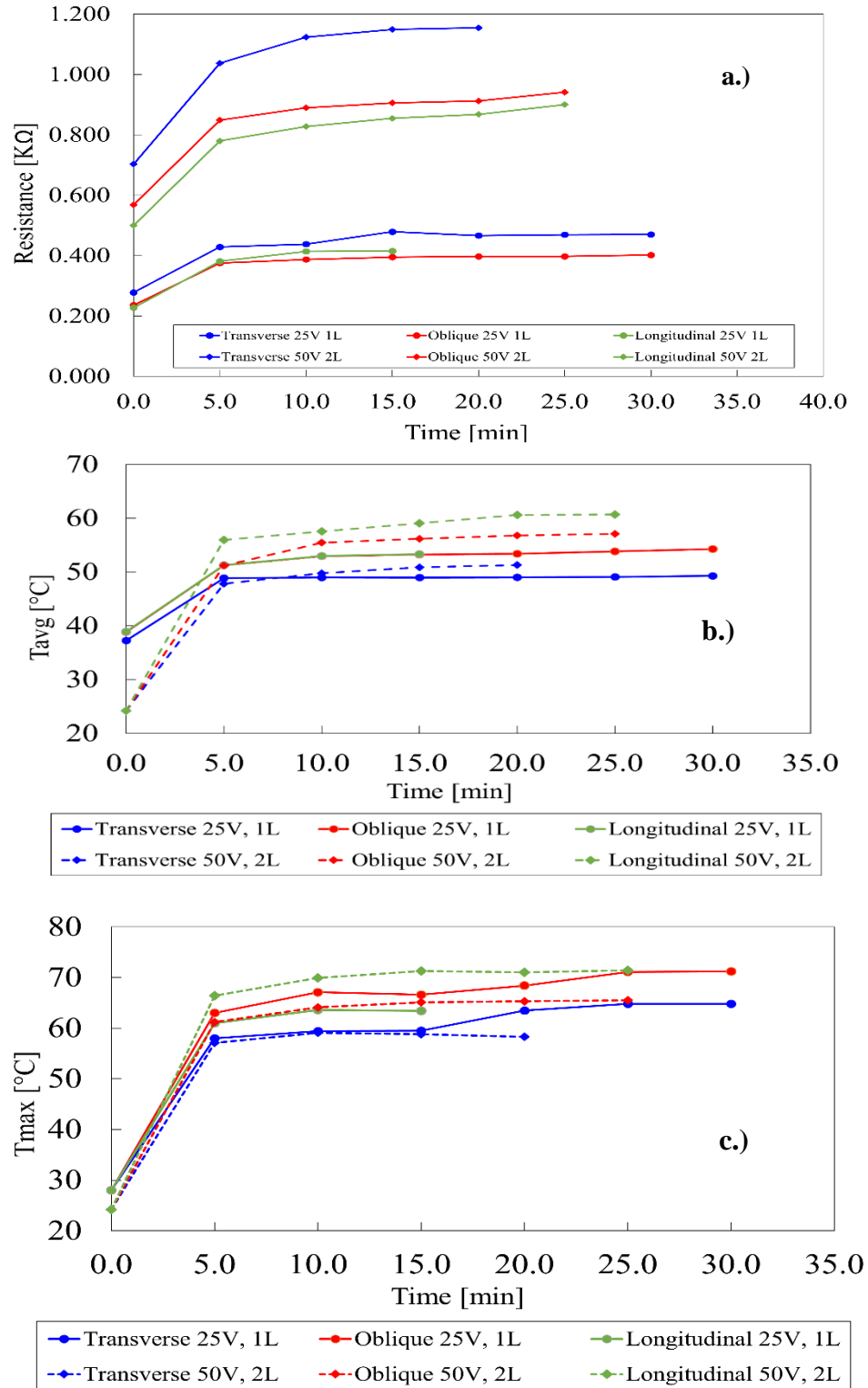


Fig. 4.9. Experimental resistance and temperature results for samples with a constant ratio of 25V/1L. This is to compare linearity and evaluate the contribution of sample length to the electrothermal behaviour of the composites. a.) Resistance vs. time. b.) Average temperature vs. time. c.) Maximum temperature vs. time.

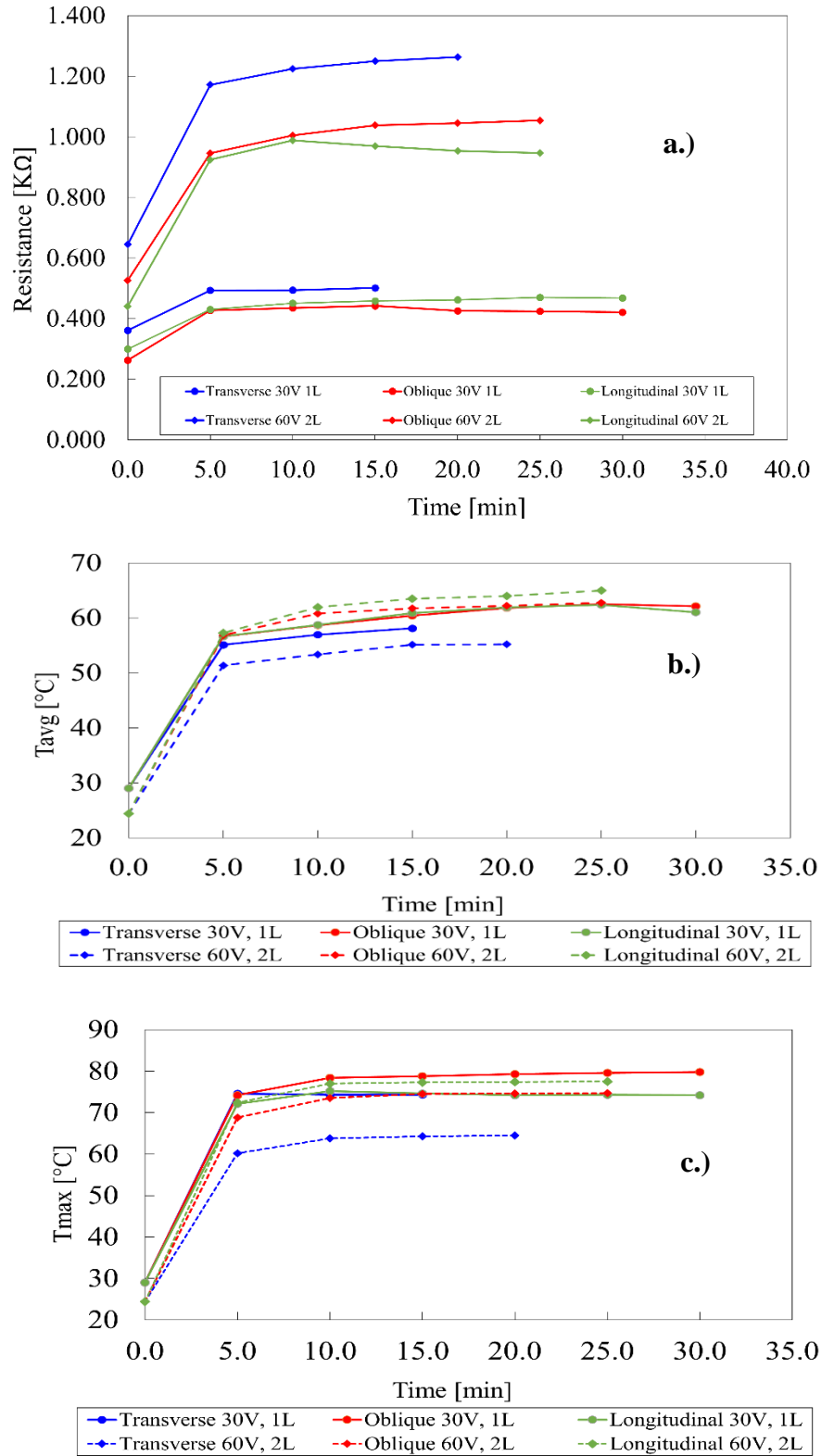


Fig. 4.10. Experimental resistance and temperature results for samples with a constant ratio of 30V/1L. This is to compare linearity and evaluate the contribution of sample length to the electrothermal behaviour of the composites. a.) Resistance vs. time. b.) Average temperature vs. time.

## Summary:

- The graphs of resistance vs. time, and temperature against time, superimposing 25V (for L samples) and 50 V (for 2L samples) curves were shown. Also, that of 30V/1L was compared with 60V/2L. Comparison with 2.75 samples will not be quite accurate since the voltage levels do not follow the x2.75 factor, except for 40V (L).
- At 40V(L) comparison could be made with 80V/2L and 110V (L); however, at 80V/2L and 110V/2.75L, the longitudinal sample was already at disequilibrium.
- Table A.3, A.4, and A.5 could be used to make the comparison of the linearity for specimens 40V/1L, 80V/2L, and 110V/2.75L.
- The transverse sample shows the lowest temperature and current value but the highest resistance value.
- The longitudinal sample exhibits the highest temperature and current value but the lowest resistance value except in 1L samples.
- Stabilization time is not drastically influenced by printing orientations or length.
- AC applied voltage contributes majorly to the stabilization time.
- The electrothermal behaviour of composites of polylactic acid with carbon black fillers is independent of sample length.
- The electrothermal response before the glass transition temperature differs from the trend after the glass transition temperature voltage.

## CHAPTER 5

### CONCLUSION

This thesis presents an analysis of the electrothermal behaviour of Polylactic acid materials reinforced with carbon black conductive particles (CB-PLA). The composite material (CB-PLA) had been subjected to AC applied voltage via joule heating. The composites were made into three prints – Transverse, Oblique, and Longitudinal, each having three length variations (1L, 2L, and 2.75L); the methodology was earlier described in chapter 3.

The result of this work affirms that PLA-based materials can contribute to limiting current consumption (waste) in electrical applications such as applications in potential protection devices (safety devices). This is due to the resistive and current behaviour of the samples as temperature increases upon imposing applied AC voltage. Also, the conductive behaviour of the composites when subjected to both low and high applied AC voltage presents the possibility of usage in energy systems, electrical, and electronics.

The foregoing objectives set at the beginning of this work were obtained. Furthermore, insights into the electrothermal behaviour of CB-PLA composite due to factors listed below were obtained.

- Applied AC Voltage: Contribution of imposed applied AC voltage on samples' behaviour
- 3D printing patterns: Influence of printing orientation.
- Glass transition temperature voltage: The electrothermal behaviour before glass transition temperature (65°C) and after the glass transition temperature.
- Geometry: Influence of length variation on the electrothermal behaviour.

For all samples, the electrical resistance and average temperature increase while the current reduces before the glass transition temperature is reached. After this temperature is reached, this trend changes. And while the temperature keeps increasing, the resistance reaches its peak and begins to drop till stabilization. Analysis of the tests showed higher resistance, least current, and least average temperature values for transverse samples (heat

dissipation reduces, obeying the Joule effect). It was clearly shown that the transverse sample exhibits the slowest thermal inertia, as this printing type did not get destabilized before longitudinal and oblique samples. This slowness in destabilization in transverse samples shows the contribution to conduction through filaments and sintering process. This is an improvement in polymeric chain mobility. This behavior of delayed destabilization in transverse samples, lasting more than ten times as long as the longitudinal destabilization, presents the property to conduct electricity and rearrange the conductive particles in the matrix at a temperature that could have destabilized its counterpart samples.

However, longitudinal samples showed the least resistance values and highest current and temperature values. The alignment of the conductive paths with the electrodes supplying the AC voltage contributed to this behaviour in the longitudinal specimen ( $0^\circ$ ). This arrangement improved the overall electric response of longitudinal samples. It could be concluded that this arrangement helps in reducing the contribution of voids along conductive filaments in PLA materials, making it suitable for applications in material science, electronics, or electrical systems.

All through this work, AC applied voltage was imposed on the samples. From the experimental result, it could be concluded that sample stabilization time is drastically influenced by AC applied voltage with respect to the glass transition temperature voltage and not the printing orientation or length. A further conclusion would be the contribution of geometry to the electrothermal behaviour of the composite samples. Results of non-linearity during the experimental analysis and comparison of the resistance and average temperature curves of 25V/1L samples with 50V/2L samples, 30V/1L samples with 60V/2L, and specimens of 40V/1L, 80V/2L, 110V/2.75L indicate an independent relationship between the electrothermal behaviour of samples (composites) and sample length.

In addition, the analyses of the  $R=R(T)$  slope (shown in chapter 4) for each length/printing exhibit a consistent electrothermal behaviour in transverse samples. Samples resistance was estimated to double as length doubles; however, the  $T_{avg}$ , and  $T_{max}$  didn't double. The overall insight of this research would contribute to further work in the field of

multifunctional conductive structures, applications in energy storage systems, wearable electronics, bioelectronics, etc.

Future directions for this work would be repeating the Joule's heating process for each printing type at a mid-voltage magnitude directly (for example, imposing an AC voltage of 50V on newly printed 2L samples) and comparing the results with that of previously degraded samples. The  $R=R(t)$  and  $T=T(t)$  curves for AC and DC applied voltage for the same length, printing, and voltage are to be obtained and compared. Also, due to inconsistencies in the result of 1L oblique samples (due to possible contributions of uncertainties during the printing process), which were supposed to have similar behaviour as 1L longitudinal samples, future experimental work would be to repeat the heating process for three oblique and three longitudinal samples of 1L to obtain the statistical deviations among curves.

## REFERENCES

- [1] F. Nadin, “When is 3D printing the best solution for production?,” *Sculpteo*, 2016. <https://www.sculpteo.com/blog/2016/05/25/when-is-3d-printing-the-best-solution-for-production/>
- [2] I. Tirado-Garcia *et al.*, “Conductive 3D printed PLA composites: On the interplay of mechanical, electrical and thermal behaviours,” *Compos. Struct.*, vol. 265, p. 113744, 2021, doi: 10.1016/j.compstruct.2021.113744.
- [3] M. Alhendi *et al.*, “Printed electronics for extreme high temperature environments,” *Addit. Manuf.*, vol. 54, p. 102709, 2022, doi: <https://doi.org/10.1016/j.addma.2022.102709>.
- [4] H. Kim and S. Lee, “Characterization of Electrical Heating of Graphene/PLA Honeycomb Structure Composite Manufactured by CFDM 3D Printer,” *Fash. Text.*, vol. 7, no. 1, p. 8, 2020, doi: 10.1186/s40691-020-0204-2.
- [5] M. Kim *et al.*, “Characterization of resistive heating and thermoelectric behavior of discontinuous carbon fiber-epoxy composites,” *Compos. Part B Eng.*, vol. 90, pp. 37–44, 2016, doi: 10.1016/j.compositesb.2015.11.037.
- [6] L. He and S.-C. Tjong, “Electrical behavior and positive temperature coefficient effect of graphene/polyvinylidene fluoride composites containing silver nanowires,” *Nanoscale Res. Lett.*, vol. 9, no. 1, p. 375, 2014, doi: 10.1186/1556-276X-9-375.
- [7] T.S. Srivatsan and T. S. Sudarshan, *Additive Manufacturing, innovations, advances and applications*. Talor & Francis Group, LLC, 2016.
- [8] S. J. Leigh, R. J. Bradley, C. P. Pursell, D. R. Billson, and D. A. Hutchins, “A Simple, Low-Cost Conductive Composite Material for 3D Printing of Electronic Sensors,” *PLoS One*, vol. 7, no. 11, p. e49365, Nov. 2012, [Online]. Available: <https://doi.org/10.1371/journal.pone.0049365>
- [9] K. Deshmukh, M. T. Houkan, M. A. AlMaadeed, and K. K. Sadasivuni, “Chapter

- 1 - Introduction to 3D and 4D printing technology: State of the art and recent trends,” K. K. Sadasivuni, K. Deshmukh, and M. A. B. T.-3D and 4D P. of P. N. M. Almaadeed, Eds. Elsevier, 2020, pp. 1–24. doi: <https://doi.org/10.1016/B978-0-12-816805-9.00001-6>.
- [10] T. Wu and B. Chen, “Facile Fabrication of Porous Conductive Thermoplastic Polyurethane Nanocomposite Films via Solution Casting,” *Sci. Rep.*, vol. 7, no. 1, p. 17470, 2017, doi: [10.1038/s41598-017-17647-w](https://doi.org/10.1038/s41598-017-17647-w).
- [11] N. li, G. Link, J. Jelonnek, and A. Heinzl, *Production of Continuous Carbon Fiber Reinforced Polyamide Filaments for Microwave Additive Manufacturing*. 2020.
- [12] Y. Zhong, R. An, H. Ma, and C. Wang, “Low-temperature-solderable intermetallic nanoparticles for 3D printable flexible electronics,” *Acta Mater.*, vol. 162, pp. 163–175, 2019, doi: <https://doi.org/10.1016/j.actamat.2018.09.069>.
- [13] P. K. Penumakala, J. Santo, and A. Thomas, “A critical review on the fused deposition modeling of thermoplastic polymer composites,” *Compos. Part B Eng.*, vol. 201, p. 108336, 2020, doi: <https://doi.org/10.1016/j.compositesb.2020.108336>.
- [14] T. QIAN, D. LIU, X. TIAN, C. LIU, and H. WANG, “Microstructure of TA2/TA15 graded structural material by laser additive manufacturing process,” *Trans. Nonferrous Met. Soc. China*, vol. 24, no. 9, pp. 2729–2736, 2014, doi: [https://doi.org/10.1016/S1003-6326\(14\)63404-X](https://doi.org/10.1016/S1003-6326(14)63404-X).
- [15] C. Zhu *et al.*, “Highly compressible 3D periodic graphene aerogel microlattices,” *Nat. Commun.*, vol. 6, no. 1, p. 6962, 2015, doi: [10.1038/ncomms7962](https://doi.org/10.1038/ncomms7962).
- [16] A. H. Loo, C. K. Chua, and M. Pumera, “DNA biosensing with 3D printing technology,” *Analyst*, vol. 142, no. 2, pp. 279–283, 2017, doi: [10.1039/C6AN02038K](https://doi.org/10.1039/C6AN02038K).
- [17] Y. Du, J. Chen, Q. Meng, J. Xu, B. Paul, and P. Eklund, “Flexible ternary carbon black/Bi<sub>2</sub>Te<sub>3</sub> based alloy/polylactic acid thermoelectric composites fabricated by additive manufacturing,” *J. Mater.*, vol. 6, no. 2, pp. 293–299, 2020, doi: [10.1039/C9JM00000A](https://doi.org/10.1039/C9JM00000A).

<https://doi.org/10.1016/j.jmat.2020.02.010>.

- [18] C. Gonçalves, I. C. Gonçalves, F. D. Magalhães, and A. M. Pinto, “Poly(lactic acid) Composites Containing Carbon-Based Nanomaterials: A Review,” *Polymers (Basel)*, vol. 9, no. 7, p. 269, Jul. 2017, doi: 10.3390/polym9070269.
- [19] R. M. Rasal, A. V. Janorkar, and D. E. Hirt, “Poly(lactic acid) modifications,” *Prog. Polym. Sci.*, vol. 35, no. 3, pp. 338–356, 2010, doi: <https://doi.org/10.1016/j.progpolymsci.2009.12.003>.
- [20] A. Rafael, L. Loong-Tak, S. Susan E.M., and T. Hideto, *Synthesis, Structures, Properties, Processing, and Applications*. San Francisco, CA, USA: John Wiley and Sons, 2010.
- [21] K. Madhavan Nampoothiri, N. R. Nair, and R. P. John, “An overview of the recent developments in polylactide (PLA) research,” *Bioresour. Technol.*, vol. 101, no. 22, pp. 8493–8501, 2010, doi: <https://doi.org/10.1016/j.biortech.2010.05.092>.
- [22] R. L. Shogren, W. M. Doane, D. Garlotta, J. W. Lawton, and J. Willett, “Biodegradation of starch/polylactic acid/poly(hydroxyester-ether) composite bars in soil,” *Polym. Degrad. Stab.*, vol. 79, pp. 405–411, Mar. 2003, doi: 10.1016/S0141-3910(02)00356-7.
- [23] J.-B. Zeng, K.-A. Li, and A.-K. Du, “Compatibilization strategies in poly(lactic acid)-based blends,” *RSC Adv.*, vol. 5, no. 41, pp. 32546–32565, 2015, doi: 10.1039/C5RA01655J.
- [24] T. Semba, K. Kitagawa, U. S. Ishiaku, and H. Hamada, “The effect of crosslinking on the mechanical properties of polylactic acid/polycaprolactone blends,” *J. Appl. Polym. Sci.*, vol. 101, no. 3, pp. 1816–1825, Aug. 2006, doi: <https://doi.org/10.1002/app.23589>.
- [25] H. Wang, X. Sun, and P. Seib, “Mechanical properties of poly(lactic acid) and wheat starch blends with methylenediphenyl diisocyanate,” *J. Appl. Polym. Sci.*, vol. 84, no. 6, pp. 1257–1262, May 2002, doi: <https://doi.org/10.1002/app.10457>.
- [26] H. Balakrishnan, A. Hassan, M. U. Wahit, A. A. Yussuf, and S. B. A. Razak,

- “Novel toughened polylactic acid nanocomposite: Mechanical, thermal and morphological properties,” *Mater. Des.*, vol. 31, no. 7, pp. 3289–3298, 2010, doi: <https://doi.org/10.1016/j.matdes.2010.02.008>.
- [27] M. E. Broz, D. L. VanderHart, and N. R. Washburn, “Structure and mechanical properties of poly(d,l-lactic acid)/poly( $\epsilon$ -caprolactone) blends,” *Biomaterials*, vol. 24, no. 23, pp. 4181–4190, 2003, doi: [https://doi.org/10.1016/S0142-9612\(03\)00314-4](https://doi.org/10.1016/S0142-9612(03)00314-4).
- [28] M. A. Abdelwahab, A. Flynn, B.-S. Chiou, S. Imam, W. Orts, and E. Chiellini, “Thermal, mechanical and morphological characterization of plasticized PLA–PHB blends,” *Polym. Degrad. Stab.*, vol. 97, no. 9, pp. 1822–1828, 2012, doi: <https://doi.org/10.1016/j.polymdegradstab.2012.05.036>.
- [29] G. H. Yew, A. M. Mohd Yusof, Z. A. Mohd Ishak, and U. S. Ishiaku, “Water absorption and enzymatic degradation of poly(lactic acid)/rice starch composites,” *Polym. Degrad. Stab.*, vol. 90, no. 3, pp. 488–500, 2005, doi: <https://doi.org/10.1016/j.polymdegradstab.2005.04.006>.
- [30] A. Pellis, E. Herrero Acero, V. Ferrario, D. Ribitsch, G. M. Guebitz, and L. Gardossi, “The Closure of the Cycle: Enzymatic Synthesis and Functionalization of Bio-Based Polyesters,” *Trends Biotechnol.*, vol. 34, no. 4, pp. 316–328, Apr. 2016, doi: [10.1016/j.tibtech.2015.12.009](https://doi.org/10.1016/j.tibtech.2015.12.009).
- [31] A. Mohammed Gumel, M. S. Annuar, and T. Heidelberg, “Current application of controlled degradation processes in polymer modification and functionalization,” *J. Appl. Polym. Sci.*, vol. 129, Sep. 2013, doi: [10.1002/app.39006](https://doi.org/10.1002/app.39006).
- [32] E. Hoveizi, M. Nabiuni, K. Parivar, S. Rajabi-Zeleti, and S. Tavakol, “Functionalisation and surface modification of electrospun polylactic acid scaffold for tissue engineering,” *Cell Biol. Int.*, vol. 38, no. 1, pp. 41–49, Jan. 2014, doi: [10.1002/cbin.10178](https://doi.org/10.1002/cbin.10178).
- [33] P. Kucharczyk *et al.*, “Functionalization of polylactic acid through direct melt polycondensation in the presence of tricarboxylic acid,” *J. Appl. Polym. Sci.*, vol.

122, no. 2, pp. 1275–1285, 2011, doi: <https://doi.org/10.1002/app.34260>.

- [34] X. Yuan *et al.*, “SURFACE MULTI-FUNCTIONALIZATION OF POLY(LACTIC ACID) NANOPARTICLES AND C6 GLIOMA CELL TARGETING in vivo,” *Chinese J. Polym. Sci.*, vol. 27, no. 02, pp. 231–239, Mar. 2009, doi: [10.1142/S0256767909003868](https://doi.org/10.1142/S0256767909003868).
- [35] V. Mittal, “Polymer Layered Silicate Nanocomposites: A Review,” *Materials*, vol. 2, no. 3. 2009. doi: [10.3390/ma2030992](https://doi.org/10.3390/ma2030992).
- [36] J.-M. Raquez, Y. Habibi, M. Murariu, and P. Dubois, “Polylactide (PLA)-based nanocomposites,” *Prog. Polym. Sci.*, vol. 38, no. 10, pp. 1504–1542, 2013, doi: <https://doi.org/10.1016/j.progpolymsci.2013.05.014>.
- [37] J.-H. Chang, Y. An, and G. Sur, “Poly(lactic acid) nanocomposites with various organoclays. I. Thermomechanical properties, morphology, and gas permeability,” *J. Polym. Sci. Part B Polym. Phys.*, vol. 41, pp. 94–103, Jan. 2003, doi: [10.1002/polb.10349](https://doi.org/10.1002/polb.10349).
- [38] M. Nofar, A. Tabatabaei, and C. B. Park, “Effects of nano-/micro-sized additives on the crystallization behaviors of PLA and PLA/CO<sub>2</sub> mixtures,” *Polymer (Guildf.)*, vol. 54, no. 9, pp. 2382–2391, 2013, doi: <https://doi.org/10.1016/j.polymer.2013.02.049>.
- [39] M. Keshtkar, M. Nofar, C. B. Park, and P. J. Carreau, “Extruded PLA/clay nanocomposite foams blown with supercritical CO<sub>2</sub>,” *Polymer (Guildf.)*, vol. 55, no. 16, pp. 4077–4090, 2014, doi: <https://doi.org/10.1016/j.polymer.2014.06.059>.
- [40] A. B., S. Suin, and B. B. Khatua, “Highly exfoliated eco-friendly thermoplastic starch (TPS)/poly (lactic acid)(PLA)/clay nanocomposites using unmodified nanoclay,” *Carbohydr. Polym.*, vol. 110, pp. 430–439, 2014, doi: <https://doi.org/10.1016/j.carbpol.2014.04.024>.
- [41] S. Singh, A. K. Ghosh, S. N. Maiti, S. Raha, R. K. Gupta, and S. Bhattacharya, “Morphology and rheological behavior of polylactic acid/clay nanocomposites,” *Polym. Eng. Sci.*, vol. 52, no. 1, pp. 225–232, Jan. 2012, doi:

<https://doi.org/10.1002/pen.22074>.

- [42] T. D. Hapuarachchi and T. Peijs, "Multiwalled carbon nanotubes and sepiolite nanoclays as flame retardants for polylactide and its natural fibre reinforced composites," *Compos. Part A Appl. Sci. Manuf.*, vol. 41, no. 8, pp. 954–963, 2010, doi: <https://doi.org/10.1016/j.compositesa.2010.03.004>.
- [43] M. A. Busolo, P. Fernandez, M. J. Ocio, and J. M. Lagaron, "Novel silver-based nanoclay as an antimicrobial in polylactic acid food packaging coatings," *Food Addit. Contam. Part A*, vol. 27, no. 11, pp. 1617–1626, Nov. 2010, doi: [10.1080/19440049.2010.506601](https://doi.org/10.1080/19440049.2010.506601).
- [44] Q. K. Meng, M. Hetzer, and D. De Kee, "PLA/clay/wood nanocomposites: nanoclay effects on mechanical and thermal properties," *J. Compos. Mater.*, vol. 45, no. 10, pp. 1145–1158, Nov. 2010, doi: [10.1177/0021998310381541](https://doi.org/10.1177/0021998310381541).
- [45] L. As'habi, S. H. Jafari, H. A. Khonakdar, R. Boldt, U. Wagenknecht, and G. Heinrich, "Tuning the processability, morphology and biodegradability of clay incorporated PLA/LLDPE blends via selective localization of nanoclay induced by melt mixing sequence," *Express Polym. Lett.*, vol. 7, pp. 21–39, 2013.
- [46] S.-M. Lai and Y.-T. Hsieh, "Preparation and Properties of Polylactic Acid (PLA)/Silica Nanocomposites," *J. Macromol. Sci. Part B*, vol. 55, no. 3, pp. 211–228, Mar. 2016, doi: [10.1080/00222348.2016.1138179](https://doi.org/10.1080/00222348.2016.1138179).
- [47] L. Basilissi, G. Di Silvestro, H. Farina, and M. A. Ortenzi, "Synthesis and characterization of PLA nanocomposites containing nanosilica modified with different organosilanes II: Effect of the organosilanes on the properties of nanocomposites: Thermal characterization," *J. Appl. Polym. Sci.*, vol. 128, no. 5, pp. 3057–3063, Jun. 2013, doi: <https://doi.org/10.1002/app.38504>.
- [48] E. Mooney *et al.*, "The electrical stimulation of carbon nanotubes to provide a cardiomimetic cue to MSCs," *Biomaterials*, vol. 33, no. 26, pp. 6132–6139, 2012, doi: <https://doi.org/10.1016/j.biomaterials.2012.05.032>.
- [49] M. Obarzanek-Fojt, Y. Elbs-Glatz, E. Lizundia, L. Diener, J.-R. Sarasua, and A.

- Bruinink, “From implantation to degradation — are poly (l-lactide)/multiwall carbon nanotube composite materials really cytocompatible?,” *Nanomedicine Nanotechnology, Biol. Med.*, vol. 10, no. 5, pp. e1041–e1051, 2014, doi: <https://doi.org/10.1016/j.nano.2013.12.012>.
- [50] G. Gorrasi, C. Milone, E. Piperopoulos, M. Lanza, and A. Sorrentino, “Hybrid clay mineral-carbon nanotube-PLA nanocomposite films. Preparation and photodegradation effect on their mechanical, thermal and electrical properties,” *Appl. Clay Sci.*, vol. 71, pp. 49–54, 2013, doi: <https://doi.org/10.1016/j.clay.2012.11.004>.
- [51] P. R. Supronowicz, P. M. Ajayan, K. R. Ullmann, B. P. Arulanandam, D. W. Metzger, and R. Bizios, “Novel current-conducting composite substrates for exposing osteoblasts to alternating current stimulation,” *J. Biomed. Mater. Res.*, vol. 59, no. 3, pp. 499–506, Mar. 2002, doi: <https://doi.org/10.1002/jbm.10015>.
- [52] B. Kumar, M. Castro, and J. F. Feller, “Poly(lactic acid)–multi-wall carbon nanotube conductive biopolymer nanocomposite vapour sensors,” *Sensors Actuators B Chem.*, vol. 161, no. 1, pp. 621–628, 2012, doi: <https://doi.org/10.1016/j.snb.2011.10.077>.
- [53] W.-M. Chiu, Y.-A. Chang, H.-Y. Kuo, M.-H. Lin, and H.-C. Wen, “A study of carbon nanotubes/biodegradable plastic polylactic acid composites,” *J. Appl. Polym. Sci.*, vol. 108, no. 5, pp. 3024–3030, Jun. 2008, doi: <https://doi.org/10.1002/app.27796>.
- [54] R. B. Ladani *et al.*, “Multifunctional properties of epoxy nanocomposites reinforced by aligned nanoscale carbon,” *Mater. Des.*, vol. 94, pp. 554–564, 2016, doi: <https://doi.org/10.1016/j.matdes.2016.01.052>.
- [55] A. Abdalla, H. H. Hamzah, O. Keattch, D. Covill, and B. A. Patel, “Augmentation of conductive pathways in carbon black/PLA 3D-printed electrodes achieved through varying printing parameters,” *Electrochim. Acta*, vol. 354, p. 136618, 2020, doi: <https://doi.org/10.1016/j.electacta.2020.136618>.

- [56] R. Taherian and Z. Samiei, "Investigation on electrical properties of polyvinyl acetate/graphite adhesive by joule heating and hall effect tests," *Mater. Today Commun.*, vol. 26, p. 101680, 2021, doi: <https://doi.org/10.1016/j.mtcomm.2020.101680>.
- [57] H. Tang, Z. Y. Liu, J. H. Piao, X. F. Chen, Y. X. Lou, and S. H. Li, "Electrical behavior of carbon black-filled polymer composites: Effect of interaction between filler and matrix," *J. Appl. Polym. Sci.*, vol. 51, no. 7, pp. 1159–1164, Feb. 1994, doi: <https://doi.org/10.1002/app.1994.070510701>.
- [58] S.-J. Park, M.-K. Seo, and J.-R. Lee, "PTC/NTC Behaviors of Nanostructured Carbon Black-filled HDPE Polymer Composites," *Carbon Lett.*, vol. 2, Jan. 2001.
- [59] W. Di and G. Zhang, "Resistivity-temperature behavior of carbon fiber filled semicrystalline composites," *J. Appl. Polym. Sci.*, vol. 91, no. 2, pp. 1222–1228, Jan. 2004, doi: <https://doi.org/10.1002/app.13281>.
- [60] R. Kumar, A. Mishra, S. Sahoo, B. P. Panda, S. Mohanty, and S. K. Nayak, "Epoxy-based composite adhesives: Effect of hybrid fillers on thermal conductivity, rheology, and lap shear strength," *Polym. Adv. Technol.*, vol. 30, no. 6, pp. 1365–1374, Jun. 2019, doi: <https://doi.org/10.1002/pat.4569>.
- [61] Q. Li, O. K. Park, and J. H. Lee, "Positive Temperature Coefficient Behavior of HDPE/EVA Blends Filled with Carbon Black," *Adv. Mater. Res.*, vol. 79–82, pp. 2267–2270, 2009, doi: [10.4028/www.scientific.net/AMR.79-82.2267](https://doi.org/10.4028/www.scientific.net/AMR.79-82.2267).
- [62] L.-R. Tan, Y.-J. Gao, S.-L. Huang, Z.-Y. Liu, and M.-B. Yang, "Factors influencing the resistivity–temperature behavior of carbon black filled isotactic polypropylene/high density polyethylene composites," *Polym. Bull.*, vol. 71, no. 6, pp. 1403–1419, 2014, doi: [10.1007/s00289-014-1131-4](https://doi.org/10.1007/s00289-014-1131-4).
- [63] A. Bairan, M. Z. Selamat, S. N. Sahadan, S. D. Malingam, and N. Mohamad, "Effect of Carbon Nanotubes Loading in Multifiller Polymer Composite as Bipolar Plate for PEM Fuel Cell," *Procedia Chem.*, vol. 19, pp. 91–97, 2016, doi: <https://doi.org/10.1016/j.proche.2016.03.120>.

- [64] A. D2734-09, “Standard test methods for void content of reinforced plastics,” *ASTM International, West Conshohocken, PA*, 2009. [www.astm.org](http://www.astm.org)
- [65] R. A. Millikan and E. S. Bishop, *Elements of Electricity*. Chicago: America Technical Society, 1917.
- [66] Fluke Corporation, “TiR2, TiR3, TiR4, Ti40, Ti45, Ti50, Ti55 IR FlexCam Thermal Imagers,” 2007. doi: <https://www.fluke.com/es-us/producto/camaras-termicas/ti55ft#>.

## APPENDIX A

TABLE A.1. EXPERIMENTAL RESULTS FOR 1L SAMPLES HEATED BY JOULE EFFECT  
IMPOSING AC VOLTAGE 25V.

VOLTAGE 25V, 1L												
Transverse					Oblique				Longitudinal			
T(min)	I(mA)	Tmax (°C)	Tavg (°C)	R(KΩ)	I(mA)	Tmax (°C)	Tavg (°C)	R(KΩ)	I(mA)	Tmax (°C)	Tavg (°C)	R(KΩ)
0	90	28	37.24	0.278	106	28	38.83	0.236	110	28	38.89	0.227
5	58.3	58	48.85	0.429	66.6	63	51.23	0.375	65.6	61	51.29	0.381
10	57.1	59.4	48.99	0.438	64.6	67.1	52.94	0.387	60.4	63.6	52.97	0.414
15	52.2	59.5	48.96	0.479	63.3	66.6	53.24	0.395	60.2	63.4	53.3	0.415
20	53.6	63.5	49.01	0.466	62.9	68.4	53.37	0.397				
25	53.3	64.8	49.07	0.469	62.9	71.1	53.82	0.397				
30	53.2	64.8	49.27	0.470	62.2	71.2	54.25	0.402				

TABLE A.2. EXPERIMENTAL RESULTS FOR 2L SAMPLES HEATED BY JOULE EFFECT  
IMPOSING AC VOLTAGE 50V.

VOLTAGE 50V, 2L												
Transverse					Oblique				Longitudinal			
T(min)	I(mA)	Tmax (°C)	Tavg (°C)	R(KΩ)	I(mA)	Tmax (°C)	Tavg (°C)	R(KΩ)	I(mA)	Tmax (°C)	Tavg (°C)	R(KΩ)
0	71.1	24.19	24.19	0.703	88	24.19	24.19	0.568	100	24.19	24.19	0.500
5	48.2	57.1	47.81	1.037	58.9	51.18	51.18	0.849	64.1	66.4	55.94	0.780
10	44.5	59.1	49.75	1.124	56.2	55.45	55.45	0.890	60.4	69.9	57.53	0.828
15	43.5	58.8	50.87	1.149	55.2	56.17	56.17	0.906	58.5	71.3	59.04	0.855
20	43.3	58.3	51.28	1.155	54.8	56.78	56.78	0.912	57.6	71	60.6	0.868
25					54.7	57.09	57.09	0.941	57.2	71.4	60.68	0.900

## APPENDIX B

TABLE A.3. EXPERIMENTAL RESULTS FOR 1L SAMPLES HEATED BY JOULE EFFECT  
IMPOSING AC VOLTAGE 40V.

VOLTAGE 40V, 1L													
Transverse					Oblique				Longitudinal				
T (min)	I (mA)	Tmax (°C)	Tavg (°C)	R(KΩ)	I (mA)	Tmax (°C)	Tavg (°C)	R(KΩ)	I (mA)	Tmax (°C)	Tavg (°C)	R(KΩ)	
0	80.1	31.2	31.2	0.499	103.5	31.2	31.2	0.386	135.3	31.2	31.2	0.296	
5	70	93.9	76.74	0.571	85.7	101.1	78.26	0.467	83.3	107	80.55	0.480	
10	83.3	98.1	78.31	0.480	98.7	107.9	84.01	0.405	86.1	111	84.31	0.465	
15	88.1	102.6	81.93	0.454	101.6	112.3	86.31	0.394	88.1	113.3	86.74	0.454	
20	89.2	106.8	83.18	0.448	102.4	117.5	89.32	0.391	92.3	115.3	89.43	0.433	
25	99.2	103.4	83.86	0.403	105.7	119.3	88.78	0.378	99.7	113.1	85.22	0.401	
30	91.9	108.3	84.42	0.435	104.3	123.1	89.04	0.384	94.3	114.3	88.93	0.424	
35	91.5	110.6	85.13	0.437	106.4	119.1	90.03	0.376	97.2	118.4	90.11	0.412	
40	91.2	114.5	85.76	0.439	106	112.6	92.78	0.377	97.1	119	92.08	0.412	
45	92.3	115.8	88.5	0.433	109.6	128.8	93.6	0.365	99	121	93.82	0.404	
50	93.3	114.8	90	0.429	111.7	128.3	94.11	0.358	99.7	120.6	94.48	0.401	
55	94	114.5	92.05	0.426	112.6	126.8	94.37	0.355	100.6	118.1	94.13	0.398	
60	93.8	114.9	93.43	0.426	112.8	126.9	95.55	0.355	103.3	125.5	95.44	0.387	

TABLE A.4. EXPERIMENTAL RESULTS FOR 2L SAMPLES HEATED BY JOULE EFFECT  
IMPOSING AC VOLTAGE 80V.

VOLTAGE 80V, 2L									
Transverse					Oblique				
T (min)	I (mA)	Tmax (°C)	Tavg (°C)	R(KΩ)	T (min)	I (mA)	Tmax (°C)	Tavg (°C)	R(KΩ)
0	115	26.8	26.8	0.696	0	186	26.8	26.8	0.430
5	54.1	76.5	63.43	1.479	5	73.3	99.4	74.06	1.091
10	53	80.3	66.44	1.509	10	71.4	101.4	77.39	1.120
15	54.9	82.2	68.59	1.457	15	73	104.5	81.38	1.096
20	56.4	83.2	70.14	1.418	20	74.1	105.6	82.73	1.080
25	57.5	83.8	72.21	1.391	25	74.8	106.4	83.2	1.070
30	58	84.9	73.44	1.379	30	75.4	107.6	83.7	1.061
35	59.1	84.4	73.95	1.354	35	76.6	108	84.83	1.044
40	59.8	85.4	74.33	1.338	40	77.9	108.7	85.42	1.027

## APPENDIX C

TABLE A.5. EXPERIMENTAL RESULTS FOR 2.75L SAMPLES HEATED BY JOULE EFFECT  
IMPOSING AC VOLTAGE 110V.

VOLTAGE 110V, 2.75L									
Transverse					Oblique				
T (min)	I (mA)	Tmax (°C)	Tavg (°C)	R(KΩ)	T (min)	I (mA)	Tmax (°C)	Tavg (°C)	R(KΩ)
0	213	31.3	31.3	0.516	0	257	31.3	31.3	0.428
5	77.9	103.9	83.72	1.412	5	92.9	119.2	91.61	1.184
10	75.9	112.1	86.95	1.449	10	90.4	119.8	96.46	1.217
15	76.5	113.3	87.88	1.438	15	90.6	123.8	98.16	1.214
20	77.2	111.6	91	1.425	20	95.9	128.8	99.61	1.147
25	77.7	113.6	92.46	1.416	25	104.3	134	100.66	1.055
30	79.1	118.8	93.4	1.391	30	106.4	130	102.72	1.034
35	80.5	118.3	93.97	1.366	35	112.2	134.1	104.36	0.980
					40	112.8	135.3	106.56	0.984
					45	115	136.5	110.36	0.965